FINITE ELEMENT ANALYSIS OF AN AXISYMMETRIC UPSETTING PROCESS

by
BHOLE JITENDRA SUDHAKAR

ME
1997
M
SUD
FIN

TH
ME/1997/M
Su22f

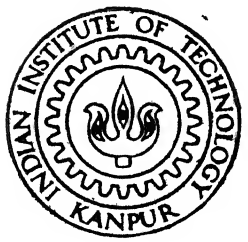

DEPARTMENT OF MECHANICAL ENGINEERING,
Indian Institute of Technology, Kanpur.
July, 1997.

FINITE ELEMENT ANALYSIS OF AN AXISYMMETRIC UPSETTING PROCESS

A THESIS SUBMITTED
IN PARTIAL FULFILLMENT OF THE REQUIREMENTS
FOR THE DEGREE OF
MASTER OF TECHNOLOGY

by
Bhole Jitendra Sudhakar

to the
DEPARTMENT OF MECHANICAL ENGINEERING
INDIAN INSTITUTE OF TECHNOLOGY
KANPUR–208016 INDIA
JULY 1997

17 AUG 1997
CENTRAL LIBRARY
I.I.T., KANPUR
No. A 123731

ME-1997-M-SUD-FIN

21.7.97

CERTIFICATE

It is certified that the work contained in the thesis entitled "***Finite Element Analysis of an Axisymmetric Upsetting Process***", by ***Bhole Jitendra Sudhakar*** , has been carried out under my supervision and that this work has not been submitted elsewhere for a degree.

P. M. Dixit

Professor

Department of Mechanical Engineering

I.I.T., Kanpur

July, 1997.

Dedicated to

My Parents

Acknowledgements

I wish to place on record my deep sense of gratitude and indebtedness to Dr. P. M. Dixit for his guidance and encouragement during the course of my thesis work.

I am thankful to Makarand, Satya, Dixitji, Hemanta and Ramesh for their active support during the course of this work. I take this opportunity to thank Girish, Maneesh, Ambarish, Avi and all others who have helped me directly or indirectly in completing this work. Finally, I thank all 'ghatmandali' for their cooperation and assistance during my stay at IIT K.

Bhole Jitendra S.

Abstract

A comprehensive analysis, of an axisymmetric upsetting process has been done to study the effects of various process variables on process parameters and deformation The process variables considered are the percent reduction in height (%r), the height to diameter ratio (H/D) and the material properties. The process parameters studied are the upsetting load, the distribution of contact normal stress at the die-workpiece interface and the contours of effective stress. The deformation is represented by the deformed mesh showing the bulge profile and the contours of effective strain. Effects of strain hardening on the process parameters and on the deformation are studied by considering two materials (aluminium and steel).

The inertial forces have been neglected. The material is assumed to be elastic-plastic strain hardening yielding according to von Mises criterion. The dies are assumed to be rigid and rough. So the process is considered under the condition of full sticking at the die-workpiece interface. The updated Lagrangian formulation which is convenient for handling geometric and material nonlinearities is used. The modified Newton-Raphson iterative scheme is used for solving the incremental equations. Validation of the model is done by comparing the results with available experimental and FEM results.

It is shown that, when a full sticking condition is used, the normal contact stress at an edge of the interface acquires an un-realistic value of infinity. Further the phenomenon of the fold-over of the free surface is observed for %r $>$ 20 or H/D $<$ 1. To avoid these things, the interfacial slip should be incorporated in the formulation. It is found that the H/D ratio does not have much influence on the process parameters. It is also observed that strain hardening doesn't affect the bulge profile or the distribution

and the values of the effective strain.

Contents

List of Figures

Nomenclature

$\{a\}$	flow vector.
A	slope of the hardening curve.
$[B_L]$	linear strain displacement matrix.
$[B_N]$	non-linear strain displacement matrix.
C_{ijkl}	fourth order elasticity tensor.
C_{ijkl}^{EP}	fourth order elastic-plastic tensor.
$[C]$	elasticity matrix.
$[C^{EP}]$	Elastic-plastic matrix.
D	diameter of the cylindrical specimen.
e_{ij}	Green-Lagrange strain tensor.
E	Young's modulus.
$\{f\}$	global internal force vector.
$\{f\}^e$	internal force vector for the element.
F	plastic potential.
$\{F\}$	global external force vector.
$\{F\}^e$	external force vector for the element.
H	height of the cylindrical specimen.
K	hardening parameter.
$[K]$	Stiffness matrix.
$[K_L]$	linear part of the stiffness matrix.
$[K_{NL}]$	non-linear part of the stiffness matrix.
n	hardening exponent.
N_i	shape function of the element.
p	hardening variable.
$\{P\}$	load vector.
$[Q]$	matrix containing the shape functions of the element.
$\underline{r}$	position vector.
R	virtual work of external forces in FE formulation.
S_{ij}	2nd Piola-Kirchoff stress tensor
t	time

u_r	displacement in r-direction.
u_z	displacement in z-direction.
$\{u\}$	displacement vector.
$\{u\}^e$	elemental displacement vector.
V	volume of the body.
δ	variation.
Δ	increment in a quantity.
ϵ_{ij}	natural strain tensor.
ϵ^e_{ij}	elastic natural strain tensor.
ϵ^p_{ij}	plastic natural strain tensor.
ϵ_{eq}	equivalent strain.
ϵ^p_{eq}	equivalent plastic strain.
$\Delta\eta_{ij}$	incremental non-linear strain tensor.
λ	scalar multiplier in flow rules.
ν	Poisson's ratio.
ρ	density.
σ_{ij}	Cauchy stress tensor.
σ'_{ij}	deviatoric part of Cauchy stress tensor.
$\overset{\circ}{\sigma}_{ij}$	Jaumann stress rate.
σ_{eq}	effective (or equivalent) stress.
σ_o	initial yield stress.
σ_y	current yield stress.
Ω_{ij}	spin tensor.

Chapter 1

Introduction

In forging, the material is squeezed between two or more dies in such a way that the metal or alloy is plastically deformed to the desired shape and size. It is also used to improve the metallurgical and mechanical properties of the material. This is the oldest of the metal working processes known to mankind since the copper age.

Generally the forging is performed by heating the material and then applying a compressive force to obtain the final shape. This is called the hot forging. The cold forging operation is carried out at room temperature. The forging operation is carried out in two different ways : drawing out and upsetting. In the drawing out operation, the metal gets elongated with a reduction in the cross-sectional area. For this purpose, the force is applied in a direction, perpendicular to the length axis. The upsetting operation is performed to increase the cross-sectional area of the material at the expense of its length. To achieve the upsetting, force is applied in a direction parallel to the length axis.

There are four types of forging methods which are generally used. They are

a. Smith forging - This is the traditional forging operation done openly or in open dies by a black smith, by manual hammering or by power hammers.

b. Drop forging - This is the operation done in closed impression dies by means of the drop hammers.

c. Press forging - Similar to drop forging, the press forging is also done in closed impression dies with the exception that the force is a continuous squeezing type applied by the hydraulic presses.

d. Machine forging - Unlike the drop or press forging where the material is drawn out, in machine forging, the material is only upset to get the desired shape.

During the application of the load in a forging operation, friction occurs at the interface of tool and workpiece. This frictional loss causes an increase in the required load. This frictional loss also depends on the length of the workpiece. In open die upsetting, due to the friction at tool-workpiece interface, the free surface of the workpiece bulges or barrels and fracture may occur at barreled surface.

1.1 Literature Survey

The problem of forging of metals has theoretical as well as technological significance in that solutions would help to bring about a better understanding of the behaviour of metals during plastic deformation at high pressure. Such solutions would give specific answers to problems actually encountered in practice. It is for these reasons that a number of investigators have dealt with the forging problem and have proposed certain theoretical solutions which are based on a material having the properties of an ideal plastic solid. This leads to so-called slip line solution. Such solutions have been proposed by Prandtl [1], Hill, Lee and Tupper [2], and Green [3]. The slip line theory has been well developed to analyse nonhomogeneous plane strain deformation of a rigid-perfectly plastic isotropic solid. This theory can be used to give very good first-approximations to loads required to perform operations and provide indications of the manner in which material deforms. However, the work hardening effects can not be incorporated in this method and therefore a detailed solution for the deformation that takes place during continued loading beyond the yield point can not be obtained using this technique. Shabaik [4] investigated the bulging in upsetting by using the slip line theory.

Hoffman and Sach [5] proposed the slab method. A complete analysis of the slab

method has been presented by Altan [6] for the axisymmetric closed die forging. In this method, a slab of infinitesimal thickness is selected and the equation representing the force equilibrium for the slab is derived, assuming that the deformation is homogeneous within the slab and that the major directions are the principal stress directions. The resulting differential equation is then solved with appropriate boundary conditions. The whole procedure is elaborate though the principle is simple . While this method can give very good predictions of the load variation with deformation, it is inherently incapable of predicting shape changes such as barreling in open die forging.

The upper bound theorem was formulated by Prager and Hodge [7]. If surfaces of velocity discontinuities are included [8], then it states that among all kinematically admissible velocity fields v_i^*, the actual one minimizes the following expression :

$$J^* = \frac{2}{\sqrt{3}} \int_V \sigma_{eq} \sqrt{0.5\, \dot{\epsilon}_{ij}^* \, \dot{\epsilon}_{ij}^*}\, dV + \int_{S_\Gamma} \tau \, |\Delta v^*| \, ds - \int_{S_t} T_i \, v_i^* \, ds$$

Here $\dot{\epsilon}_{ij}^*$ is the strain rate field derived from v_i^* and $|\Delta v^*|$ denotes the discontinuity in the tangential components of the velocity across the surface S_Γ. Further, σ_{eq} represents the equivalent stress, τ denotes the shear stress on the surface of discontinuity S_Γ and T_i is the specified traction on the surface S_t. The first term expresses the power spent in causing the internal deformation over the volume V of deforming body. The second term represents the power loss over the surfaces of velocity discontinuities including the boundary between tool and material. The last term represents the power supplied by specified tractions. What the upper bound theorem states is that the actual externally supplied power is never higher than that computed by using above equation.

Kudo [9] applied the upper bound theorem to the problem of axisymmetric cold forging and extrusion. Here, he examined two types of admissible velocity fields. He introduced the conception of a unit cylindrical deforming region to simplify the analysis of complicated problems. Upper bound solutions for problems with Coulomb's friction, non-steady processes and work hardening material are also included in this paper. Kudo [10] also applied the upper bound theorem to the analysis of the plane strain forging and extrusion. Avitzur [11], S. Kobayashi [12], McDonald, Kobayashi and Thomsen [13], Kobayashi and Thomsen [14,15], Liu [16] and many others have suggested upper bound velocity fields to predict the forming load in upsetting with bulging.

The major difficulty in using the upper bound method is how to choose the kinematically admissible velocity field since the accuracy of the solution depends on how close the assumed velocity field is to the actual one.

Accurate determination of forging parameters under realistic conditions became possible when the finite element method (FEM) was introduced. The major advantage of the finite element method is that the method can be applied to a wide class of boundary value problems without restrictions of workpiece geometry. This is achieved by the proper discretization procedure used in the finite element method. Using FEM, it is possible to predict the platen forces, the pressure distributions, the strain (i. e. metal flow) and hardness distributions within the billet, for various deformation levels of interface shear stress.

Early applications of the FEM to forging problems were based on the incremental method proposed by Lee and Kobayashi [17]. The method uses the elastic-plastic stress-strain matrix based on the Generalised Hooke's law and the Prandtl-Reuss equations. The additivity of incremental elastic and plastic strains is assumed. Even though the stress-strain matrix and the geometry are updated after every increment, only the linearised incremental equations are used. The method was applied to solid cylinder upsetting [18], ring compression [19] and for predicting defects in upsetting [20]. Lee and Kobayashi [21] studied the problem of simple upsetting with complete sticking at the tool-workpiece interface using the method. Maccarini et al [22] used the method for studying the influence of die geometry on cold extrusion forging operation. Whereas Lee and Kobayashi [17] used the velocity as the primary unknown; Hartley et al [23] proposed an incremental method with the displacement as the primary unknown. In their method also, the linearised incremental equations are used and the elastic-plastic matrix and the geometry are updated after every increment. They studied the the upset forging process using the method where the interfacial friction has been incorporated using the β-stiffness method [24].

Linearised incremental equations give only an approximate solutions. If the incremental size is not sufficiently small, the error between the exact and the approximate solutions grows rapidly with the applied load, as the error in the solution of the current increment gets propogated into the next increment when the stress-strain matrix

and the geometry are updated. To avoid this phenomenon, the non-linear incremental equations should be solved by using a scheme like Newton-Raphson scheme. Such a formulation was first proposed by Bathe [25]. The updated Lagrangian formulation of Bathe [25] has been applied by Carter and Lee [26] to axisymmetric upsetting. The thrust of the work of Carter and Lee [26], however, has been towards studying the interface mechanics rather than analysing the axisymmetric upsetting. They have used the contact surface algorithm to enforce the friction condition (Coulomb's law) at the interface.

Even though a lot of finite element studies have been carried out on axisymmetric upsetting, most of them have used linearised incremental equations without using sufficiently small incremental size. As a result, these analyses are approximate . There is a need to carry out a more accurate analysis of the process using the updated Lagrangian formulation with a Newton-Raphson iterative scheme for solving the incremental equations. This is the objective of the present study. Of course, for an accurate analysis, the interfacial friction also needs to be modelled properly. This requires development of an appropriate contact algorithm. However, due to lack of time, this part of the work could not be carried out.

1.2 Modelling of Cold Forging Process

In the present work, the process of cold upsetting of cylindrical solid disk is studied. The process is considered to be axisymmetric. The updated Lagrangian formulation which is convenient for handling geometric and material nonlinearities is used. Newton-Raphson iterative scheme is used for solving the incremental equations. The material is assumed to be elastic-plastic strain hardening yielding according to von Mises criterion. The effects of temperature and strain rate (viscoplasticity effects) on the yield strength of the material are ignored in this work. The inclusion of these effects renders the analysis quite complex. Due to small acceleration, inertial forces are not included. The body forces are also neglected.

The dies are assumed to be rigid and rough. So no relative displacement is permitted at the tool-workpiece interface and the process is considered under condition

of complete sticking at the tool-workpiece interface.

1.3 Objective

In the present work, a finite element code for a large deformation elastic -plastic problem is developed using the updated Lagrangian formulation of Bathe [25]. The code is developed for displacement controlled problems.

First, the code is validated by comparing the results with experimental as well as FEM results of reference [21]. Then, a detailed parametric study is carried out to show the effects of three process variables namely the percentage reduction in height (% r), the height to diameter ratio (H/D) and the material properties. The parameters considered are the forging load, the contact normal stress distribution at the tool-workpiece interface, the effective stress and strain contours and some deformation patterns.

The deformation pattern is studied using the deformed mesh or the bulging profiles of free surfaces of the cylindrical solid work- piece. The prediction of the metal flow in the workpiece is done by using the contours of the effective strain.

1.4 Plan of the Thesis

The thesis is organised as follows :

In the second chapter, the updated Lagrangian method for problem with geometric and material nonlinearities and the corresponding finite element formulation are presented. The application of the boundary conditions and the solution procedure for the problem of cold upsetting are discussed at the end.

In chapter 3, the results obtained by applying the method for a range of cases are presented along with the comparison with experimental results and a discussion on the parametric study.

Conclusions and suggestions for further work are discussed in chapter 4.

Chapter 2

Mathematical Modelling of an Axisymmetric Upsetting Process

In this chapter, the mathematical model for cold upsetting process is developed The process is modelled as a steady state axi-symmetric problem. The constitutive equation for the mechanical behavior of the work material is stated. The interaction between the work and it's surrounding are represented by appropriate boundary conditions. The finite element method formulation is presented at the end of this chapter.

2.1 Governing Equations

In the study of the deformation of a body subjected to external loading, often the original undeformed and unstressed state of the body is used for the formulation of its equation of motion: This is known as *Lagrangian Formulation.* This formulation is convenient for *small deformation* which is the case in a majority of engineering problems. In such cases, the deformed configuration does not deviate much from the original one and hence the deformation can be described by an infinitesimal strain tensor, known as the engineering strain tensor, for which the strain-displacement relation is *linear.*

On the other hand, for *large deformation* problems one has to use a finite strain measure which is expressed by a non-linear strain-displacement relation. Furthermore,

the equations of motion of the reference configuration depend on the deformation. Hence, for all large deformation problems the Lagrangian Formulation proves to be cumbersome with the governing equations being difficult to solve. In such cases, one solves the problem using an incremental method known as *Updated Lagrangian Formulation*. In this formulation, it is assumed that the state of the stress and deformation of the body is known till the current configuration, say at time t. The main objective is to determine the incremental deformation and stresses during an infinitesimal time step $\mathrm{d}t$, i. e. from time t to $t + \mathrm{d}t$. Here, the current configuration is used as the reference configuration for obtaining the incremental values. Unlike the Lagrangian Formulation, an incremental strain tensor is used. The methodology is particularly useful for elastic-plastic materials because the stress-strain relationship in such materials is usually expressed in an incremental fashion.

2.1.1 Strain-Displacement Relations

Figure (2.1) shows a body in its current configuration (which is being used as the reference configuration) at time t and a possible deformed configuration at time $t+\Delta t$. The vectors $\underline{u}^t$ and $\underline{u}^{t+\Delta t}$ denote the displacements of a point P of the body at time t and $t + \Delta t$, respectively. The position vectors of P at the above times are depicted as $\underline{r}^t$ and $\underline{r}^{t+\Delta t}$, respectively. For a very small value of Δt, one can represent it as $\mathrm{d}t$. Thus , from the figure it can be seen that $\underline{\mathrm{d}u}$ is the incremental displacement of P for the time step $\mathrm{d}t$. For small incremental deformation, one can represent it tensorially using the following linear incremental strain tensor:

$$\mathrm{d}\epsilon_{ij} = \frac{1}{2}\left(\mathrm{d}u_{i,j} + \mathrm{d}u_{j,i}\right) \tag{2.1}$$

Note that $\mathrm{d}\epsilon_{ij}$ is not the incremental engineering strain tensor but the incremental logarithmic or natural strain tensor.

If the incremental deformation is large, the incremental strain-displacement relationship has to be non-linear, i. e. :

$$\mathrm{d}e_{ij} = \frac{1}{2}\left(\mathrm{d}u_{i,j} + \mathrm{d}u_{j,i} + \mathrm{d}u_{k,i}\mathrm{d}u_{k,j}\right) \tag{2.2}$$

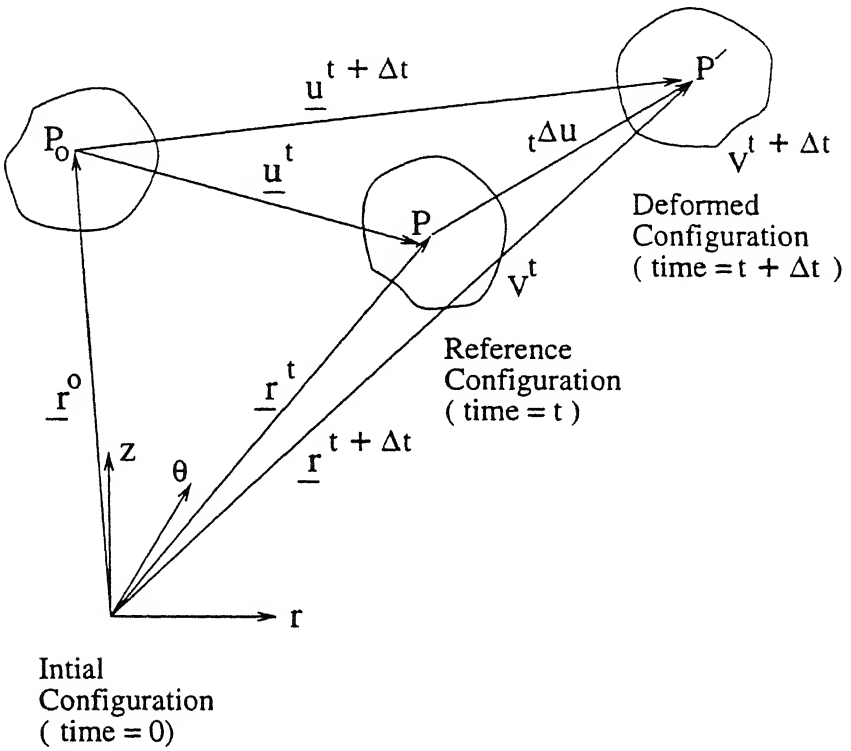

Figure 2.1: Configuration

The tensor de_{ij} is known as *Green Lagrange strain tensor*. Henceforth, it is assumed that the incremental displacement is small and thus the linear strain-displacement relation given by eq. (2.1) holds true.

2.1.2 Constitutive Equations

The plastic part of the incremental stress-strain relationship is obtained from the plastic potential of the material. For a material, yielding according to the von Mises criterion in an isotropic fashion, the plastic potential is given by [27],

$$F(\sigma_{ij}, p) = \sigma_{eq}(\sigma_{ij}) - \sigma_y(p) \tag{2.3}$$

Note that

$$F = 0 \tag{2.4}$$

represents the yield criterion. The plastic potential F depends on the Cauchy stress tensor σ_{ij} through it's second invariant σ_{eq} called as equivalent stress and defined by

$$\sigma_{eq} = (\frac{3}{2}\sigma'_{ij}\sigma'_{ij})^{\frac{1}{2}} \tag{2.5}$$

where σ'_{ij} is the deviatoric part of σ_{ij}. Further, F depends on the variable yield stress of the material, σ_y , through a hardening variable p. For the case of strain hardening, p is identified as the equivalent plastic strain ϵ^p_{eq}, and hence defined as :

$$p = \epsilon^p_{eq} = \int \mathrm{d}\epsilon^p_{eq} \tag{2.6}$$

and

$$\mathrm{d}\epsilon^p_{eq} = (\frac{2}{3}\mathrm{d}\epsilon^p_{ij}\mathrm{d}\epsilon^p_{ij})^{\frac{1}{2}} \tag{2.7}$$

Here, $\mathrm{d}\epsilon^p_{ij}$ is the plastic part of the incremental strain tensor $\mathrm{d}\epsilon_{ij}$ and the integration in eq.(2.6) is to be carried along the particle path.The dependence of σ_y on p (or ϵ^p_{eq})is normally approximated by a power-law type of relationship

$$\sigma_y = K(\epsilon^p_{eq})^n \tag{2.8}$$

Here, K is called the hardening coefficient and n is called as the hardening exponent.

The incremental plastic strain ($\mathrm{d}\epsilon^p_{ij}$) is obtained from the plastic potential using the following relation :

$$\mathrm{d}\epsilon^p_{ij} = \mathrm{d}\lambda\frac{\partial F}{\partial \sigma_{ij}} \tag{2.9}$$

where $\mathrm{d}\lambda$ is a scalar. This equation is called as the flow rule. Differentiation of eq.(2.3) with respect to σ_{ij} gives

$$\frac{\partial F}{\partial \sigma_{ij}} = \frac{3}{2\sigma_{eq}}\sigma'_{ij} \tag{2.10}$$

Using this and from eq.(2.9), one can determine $\mathrm{d}\lambda$ as:

$$\mathrm{d}\lambda = \mathrm{d}\epsilon^p_{eq} \tag{2.11}$$

Further, the hardening relationship and the yield condition (eq. 2.4) can be used to express $\mathrm{d}\lambda$ as :

$$\mathrm{d}\lambda = \frac{\mathrm{d}\sigma_y}{H} = \frac{\mathrm{d}\sigma_{eq}}{H} \tag{2.12}$$

where

$$H = \frac{d\sigma_{ij}}{d\epsilon^p_{eq}}, \tag{2.13}$$

the slope of the hardening curve, can be obtained from eq. (2.8). Substitution of eqs. (2.10) and (2.12) in eq. (2.9) leads to the following constitutive equation

$$d\epsilon^p_{ij} = \frac{3}{2}\frac{d\sigma_{eq}}{H\sigma_{eq}}\sigma'_{ij} \tag{2.14}$$

This constitutive relationship between the deviatoric stress tensor and the incremental plastic strain tensor is not really convenient for an updated Lagrangian formulation for which the incremental stress-strain relationship is needed. This can be obtained from eq. (2.14) as follows:

$$d\epsilon^p_{ij} = \frac{3}{2}\frac{\sigma'_{ij}}{H\sigma_{eq}}\frac{\partial\sigma_{eq}}{\partial\sigma_{kl}}d\sigma_{kl} \tag{2.15}$$

Note that,from eqs. (2.3) and (2.10), we get

$$\frac{\partial\sigma_{eq}}{\partial\sigma_{kl}} = \frac{\partial F}{\partial\sigma_{kl}} = \frac{3}{2\sigma_{eq}}\sigma'_{kl}. \tag{2.16}$$

Substitution of eq. (2.16) in eq. (2.15) leads to the following incremental plastic stress-strain relationship :

$$d\epsilon^p_{ij} = \frac{9\sigma'_{ij}\sigma'_{kl}}{4H\sigma^2_{eq}}d\sigma_{kl}. \tag{2.17}$$

The incremental elastic stress-strain relationship is given by

$$d\epsilon^e_{ij} = \frac{1}{E}[-\nu d\sigma_{kk}\delta ij + (1+\nu)d\sigma_{ij}] \tag{2.18}$$

where $d\epsilon^e_{ij}$ is the elastic part of $d\epsilon_{ij}$, E is the Young's modulus and ν is the Poisson's ratio. Adding the two relationships, we get

$$\begin{aligned} d\epsilon_{ij} &= d\epsilon^e_{ij} + d\epsilon^p_{ij} \\ &= \left[-\frac{\nu}{E}\delta_{ij}\delta_{kl} + \frac{(1+\nu)}{E}\delta_{ik}\delta_{jl} + \frac{9\sigma'_{ij}\sigma'_{kl}}{4H\sigma^2_{eq}}\right] d\sigma_{kl} \end{aligned} \tag{2.19}$$

This is the incremental elastic-plastic stress-strain relationship needed in the updated Lagrangian formulation. However, it is the following inverse relationship [28] which is more useful :

$$d\sigma_{ij} = C^{EP}_{ijkl} d\epsilon_{kl} \tag{2.20}$$

where

$$C^{EP}_{ijkl} = 2\mu \left[\delta_{ik}\delta_{jl} + \frac{\nu}{1-2\nu}\delta_{ij}\delta_{kl} - \frac{9\mu \sigma'_{ij}\sigma'_{kl}}{2(3\mu + H)\sigma^2_{eq}} \right] \tag{2.21}$$

and μ is the shear modulus related to E and ν by the relation:

$$\mu = \frac{E}{2(1+\nu)} \tag{2.22}$$

In eq (2.20), if the increment consists of only a pure rigid rotation, then $d\sigma_{ij}$ must be zero. Such a stress increment is called an *objective* stress increment. Thus, in the incremental elastic-plastic stress-strain relationship (eq. 2.20), the incremental stress tensor must be an objective stress tensor. The Cauchy stress tensor does not satisfy the objective requirement. So $d\sigma_{ij}$ in eq. (2.20) can not be interpreted as the incremental Cauchy stress-tensor. The two most commonly used objective stress tensors are (i) the *2nd Piola-Kirchoff* stress tensor S_{ij}, (ii) stress tensor whose material time derivative is given by the *Jaumann stress rate* $\overset{\circ}{\sigma}_{ij}$. If we use the latter, then $d\sigma_{ij}$ in eq. (2.20) should be identified as $\overset{\circ}{\sigma}_{ij}\, dt$. Thus

$$\overset{\circ}{\sigma}_{ij}\, dt = C^{EP}_{ijkl} d\epsilon_{kl} \tag{2.23}$$

The Jaumann rate $\overset{\circ}{\sigma}_{ij}$ is related to Cauchy rate $\dot{\sigma}_{ij}$ by the relation

$$\overset{\circ}{\sigma}_{ij}\, dt = \dot{\sigma}_{ij} dt - \sigma_{ik}(\Omega_{jk} dt) - \sigma_{jk}(\Omega_{ik} dt) \tag{2.24}$$

where the incremental rotation tensor $(\Omega_{ij} dt)$ is defined as

$$\Omega_{ij} dt = \frac{1}{2}(du_{i,j} - du_{j,i}). \tag{2.25}$$

Equations (2.21, 2.23-2.25) represents the elastic-plastic incremental stress-strain relationship to be used in the updated Lagrangian formulation.

2.1.3 Equilibrium Equations

In the upsetting, we assume that the load is applied slowly so that the resulting accelerations are very small. Then, the inertial forces become negligible and the problem can be treated as a static problem. Neglecting body forces also, the equilibrium equation becomes

$$\sigma_{ij,j} = 0. \tag{2.26}$$

This equation is to be satisfied in the deformed configuration (i. e. in the configuration at time t+dt) which is not known yet. In updated Lagrangian formulation, we need equilibrium equation in terms of the incremental stress. The incremental form of eq. (2.26) is given by [29]:

$$\mathrm{d}\sigma_{ij,j} - (\sigma_{ij,k})\mathrm{d}u_{k,j} = 0. \tag{2.27}$$

Note that $\mathrm{d}\sigma_{ij}$ in the above equation is the incremental Cauchy stress tensor and hence equal to $\dot{\sigma}_{ij}\mathrm{d}t$.

Now the above equations can be collected together to define the updated Lagrangian formulation.

2.1.4 Updated Lagrangian Formulation

It is assumed that the net load is applied in several increments and after a certain number of increments, we arrive at the current configuration (i. e. the configuration at the present time t), which is treated as the reference configuration. Further, the displacement vector u_i and the stress tensor σ_{ij} at the present time are known. Now a load increment is applied to the current configuration. Then to find the resulting incremental displacements, strains and stresses $(\mathrm{d}u_i, \mathrm{d}\epsilon_{ij}, \mathrm{d}\sigma_{ij})$, we have to solve the following equations:

(a) Incremental equilibrium equations:

$$\mathrm{d}\sigma_{ij,j} - (\sigma_{ij,k})\mathrm{d}u_{k,j} = 0; \tag{2.28}$$

(b) Incremental stress-strain relations:

$$\overset{\circ}{\sigma}_{ij}\, \mathrm{d}t = C^{EP}_{ijkl} \mathrm{d}\epsilon_{kl}; \tag{2.29}$$

[$\overset{\circ}{\sigma}_{ij}$ defined by eqs. (2.24-2.25) and C^{EP}_{ijkl} defined by eq. (2.21)]

(c) Incremental strain-displacement relations:

$$\mathrm{d}\epsilon_{ij} = \frac{1}{2}(\mathrm{d}u_{i,j} + \mathrm{d}u_{j,i}) \tag{2.30}$$

Note : When the incremental deformation is large, the non-linear incremental strain displacement relation (eq. 2.2) should be used.

2.2 Boundary Conditions

The typical boundary conditions are as follows:
(i) *Geometric* or *essential* boundary conditions.
The incremental displacement vector is specified at a point on the boundary.

(ii) *Force* or *natural* boundary conditions.
The incremental stress vector $\mathrm{d}t_i = \mathrm{d}\sigma_{ij}\, n_j$ is specified at a point on the boundary, where n_j represents the components of the unit outward normal vector.

Sometimes, we have mixed boundary conditions, i. e. at a point on the boundary, some incremental displacement components and the remaining components of the incremental stress vector are specified.

Figure 2.2 shows the domain of the problem. Due to the symmetry, only the upper right quarter of the work piece is used for analysis.

The boundary conditions for the domain of our problem are discussed below:

(i) The workpiece-die interface (AB):

Because of assumption of complete sticking condition at the workpiece- die interface, the component of incremental displacement in r-direction is zero. Also, since

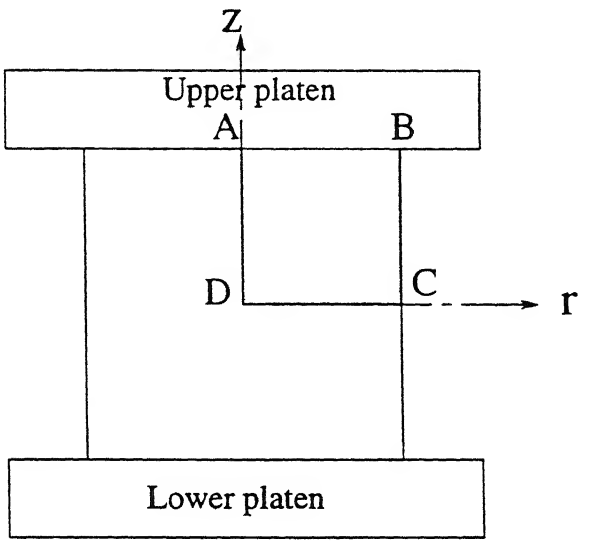

Figure 2.2: Compression of a cylindrical solid disk between two platens

our problem is displacement controlled, the incremental displacement component in the z-direction is specified.

Thus, the boundary conditions on AB are

Essential boundary conditions:

$$\mathrm{d}u_r = 0,\ \mathrm{d}u_z = specified \tag{2.31}$$

(ii) The free surface (BC):

Since this boundary is a free surface, it is traction free. When the workpiece comes in contact with the die , this surface bulges. Therefore, the components of incremental displacement $\mathrm{d}u_r$ and $\mathrm{d}u_z$ can not be assumed to be zero. Thus, the boundary conditions on BC are :

Natural boundary conditions:

$$\mathrm{d}t_z = \mathrm{d}\sigma_{rz} = 0 \tag{2.32}$$

and

$$\mathrm{d}t_r = \mathrm{d}\sigma_{rr} = 0$$

(iii) The plane of symmetry (CD):

Because of symmetry, the z-component of incremental displacement and r-component of incremental stress vector are zero. So we have the following boundary conditions on CD:

Natural Boundary Condition:

$$\mathrm{d}t_r = \mathrm{d}\sigma_{rz} = 0 \tag{2.33}$$

Essential Boundary Condition:

$$\mathrm{d}u_z = 0 \tag{2.34}$$

(iv) The axis of symmetry, z-axis (DA) : Again, because of symmetry, the r-component of incremental displacement and z-component of incremental stress vector are zero on DA. Therefore, the boundary conditions on DA are

Natural Boundary Condition:

$$\mathrm{d}t_z = \mathrm{d}\sigma_{rz} = 0 \tag{2.35}$$

Essential Boundary Condition:

$$\mathrm{d}u_r = 0 \tag{2.36}$$

2.3 Finite Element Formulation

In this section, a finite element formulation corresponding to the updated Lagrangian approach of section 2.1 has been developed. First, an elastic-plastic matrix relating incremental stress and strain vectors is derived using the plastic potential proposed in section 2. 1. Then, the equilibrium equations in the deformed configuration are derived using the principle of virtual work following a procedure given in [25]. Finally, the numerical scheme required to implement the finite element formulation, is discussed.

2.3.1 Incremental Stress-Strain Relationship Representing Material Non-linearity

Since the stress-strain relationship is path dependent for an elastic-plastic material, it is convenient to represent it in incremental form. The incremental stress-strain relation is expressed in vector form as

$$\{\mathrm{d}\sigma\} = [C]^{EP}\{\mathrm{d}\epsilon\} \tag{2.37}$$

where

$$\{\mathrm{d}\sigma\}^T = \{\mathrm{d}\sigma_{rr}, \mathrm{d}\sigma_{zz}, \mathrm{d}\sigma_{rz}, \mathrm{d}\sigma_{\theta\theta}\} \tag{2.38}$$

and

$$\{\mathrm{d}\epsilon\}^T = \{\mathrm{d}\epsilon_{rr}, \mathrm{d}\epsilon_{zz}, 2\mathrm{d}\epsilon_{rz}, \mathrm{d}\epsilon_{\theta\theta}\} \tag{2.39}$$

are respectively the vector forms of the incremental (objective) stress and strain tensors The expression for the elastic-plastic matrix $[C^{EP}]$ is derived from the plastic potential F. For its derivation, it is convenient to express the yield condition eqs. (2.3) and (2.4) as

$$F(\{\sigma\}, p) \equiv \sigma_{eq}(\{\sigma\}) - \sigma_y(p) = 0 \tag{2.40}$$

where

$$\{\sigma\}^T = \{\sigma_{rr}, \sigma_{zz}, \sigma_{rz}, \sigma_{\theta\theta}\} \tag{2.41}$$

On the yield surface, $\mathrm{d}F = 0$ and hence

$$(\frac{\partial F}{\partial\{\sigma\}})^T\{\mathrm{d}\sigma\} + \frac{\partial F}{\partial p}\mathrm{d}p = 0 \tag{2.42}$$

or

$$\{a\}^T\{\mathrm{d}\sigma\} - A\mathrm{d}\lambda = 0 \tag{2.43}$$

where, the flow vector $\{a\}$ is defined by

$$\{a\} = \frac{\partial F}{\partial\{\sigma\}}, \tag{2.44}$$

the parameter A is given by

$$A = -\frac{1}{\mathrm{d}\lambda}\frac{\partial F}{\partial p}\mathrm{d}p, \tag{2.45}$$

and $d\lambda$ is the same scalar which appears in eq. (2.9). Eq. (2.10) gives the following expression for the flow vector:

$$\{a\} = \frac{3}{2\sigma_{eq}}\{\sigma\}'. \tag{2.46}$$

where $\{\sigma\}'$ is the vector form of the deviatoric part of σ_{ij}. Eqs. (2.6) and (2.11) give

$$dp = d\lambda = d\epsilon^p_{eq}. \tag{2.47}$$

Substitution of eqs. (2.40) and (2.47) in eq. (2.45) leads to the following expression for A:

$$A = \frac{d\sigma_y}{dp} = \frac{d\sigma_y}{d\epsilon^p_{eq}} \tag{2.48}$$

The total strain increment can be split into elastic and plastic parts. Thus

$$\{d\epsilon\} = \{d\epsilon^e\} + \{d\epsilon^p\} = [C]^{-1}\{d\sigma\} + d\lambda\frac{\partial F}{\partial\{\sigma\}}$$

$$= [C]^{-1}\{d\sigma\} + d\lambda\{a\} \tag{2.49}$$

Here, $[C]$ is the matrix form of the elasticity tensor C_{ijkl} (See eq. 2.18). The second part of the right hand of eq. (2.49) is due to the flow rule (eq. 2.9). Premultiplying both sides of equation (2.49) by $\{a\}^T[C]$ and using eq. (2.43) , we get

$$d\lambda = \frac{\{a\}^T[C]\{d\epsilon\}}{A + \{a\}^T[C]\{a\}} \tag{2.50}$$

Substituting the above expression for $d\lambda$ in eq. (2.49), we get

$$\{d\epsilon\} = [C]^{-1}\{d\sigma\} + \frac{\{a\}^T[C]\{d\epsilon\}}{A + \{a\}^T[C]\{a\}}\{a\} \tag{2.51}$$

which leads to

$$\{d\sigma\} = \left([C] - \frac{[C]\{a\}\{a\}^T[C]}{A + \{a\}^T[C]\{a\}}\right)\{d\epsilon\} \tag{2.52}$$

Therefore,

$$[C]^{EP} = \left([C] - \frac{[C]\{a\}\{a\}^T[C]}{A + \{a\}^T[C]\{a\}}\right) \tag{2.53}$$

where the expression for $\{a\}$ is given by eq. (2.46). For a material with power strain hardening law (eq. 2.8), the expression (2.48) for A reduces to

$$A = K\,n(\epsilon^p_{eq})^{n-1} \tag{2.54}$$

For an isotropic material, the expression for $[C]$ for the axisymmetric case is given by

$$[C] = \frac{E}{(1+\nu)(1-2\nu)} \begin{bmatrix} 1-\nu & \nu & 0 & \nu \\ \nu & 1-\nu & 0 & \nu \\ 0 & 0 & \frac{1-2\nu}{2} & 0 \\ \nu & \nu & 0 & 1-\nu \end{bmatrix} \tag{2.55}$$

As stated at the end of subsection 1.1.2, the vector $\{d\sigma\}$ in eq. (2.52) should be interpreted as an objective stress increment.

2.3.2 Updated Lagrangian Formulation for Geometric Non-Linearity

When a body experiences a large deformation and/or rotation, the equilibrium must be established in the current configuration. The normal solution procedure adopted in this case is updated Lagrangian. That is to say that when all the kinematical variables are known from time 0 to time t in discreate time steps, the objective is to establish the equilibrium in the configuration at time $t+\Delta t$. In order to derive the finite element equilibrium equations at time $t + \Delta\, t$, the principle of virtual work requires that

$$\int_{V^{t+\Delta t}} \sigma_{ij}^{t+\Delta t}\, \delta(\epsilon_{ij}^{t+\Delta t})\, dV^{t+\Delta t} = R^{t+\Delta t} \tag{2.56}$$

where $\sigma_{ij}^{t+\Delta t}$ is the Cauchy stress tensor at time $t+\Delta t$, $\delta(\epsilon_{ij}^{t+\Delta t})$ is the virtual infinitesimal strain tensor at time $t + \Delta t$, $R^{t+\Delta t}$ is the virtual work of the surface forces at time $t + \Delta t$ (body forces being neglected) and $V^{t+\Delta t}$ is the domain at time $t + \Delta t$. The major difficulty in application of eq. (2.56) is that the configuration at $t + \Delta t$ is unknown. Morever quantities like Cauchy stress tensor are not purely additive as one has to take care of rotation into account.

An elegant way of formulating the problem is given by Bathe [25]. Here, the virtual work expression (eq. 2.56) is transformed to an integral over the known domain at time t (i. e. V_t) using the 2nd Piola- Kirchoff stress tensor and the Green-Lagrange strain tensor. Thus, the virtual work expression becomes

$$\int_{V_t} {}_tS_{ij}^{t+\Delta t}\, \delta({}_te_{ij}^{t+\Delta t})\, dV^t = R^{t+\Delta t}. \tag{2.57}$$

where S_{ij} denotes the 2nd Piola- Kirchoff stress tensor whose relation with the Cauchy stress tensor σ_{ij} is given by

$$ {}_tS_{ij}^{t+\Delta t} = \frac{\rho^t}{\rho^{t+\Delta t}} ({}_{t+\Delta t}r_{i,m}^t)\, \sigma_{mn}^{t+\Delta t} ({}_{t+\Delta t}r_{j,n}^t). \tag{2.58} $$

[The right superscript stands for the current configuration and the left subscript denotes the reference configuration.]

Since the Cauchy stress tensor is always referred to the current configuration, the left subscript has been omitted. Here ${}_{t+\Delta t}r_{i,m}^t$ represents the derivative of the position vector $\underline{r}^t$ at time t with respect to the one ($\underline{r}^{t+\Delta t}$) at time $t+\Delta t$ and $\frac{\rho^t}{\rho^{t+\Delta t}}$ denotes the ratio of densities at time t and $t+\Delta t$. The Green-Lagrange strain tensor ${}_te_{ij}^{t+\Delta t}$ is defined as

$$ {}_te_{ij}^{t+\Delta t} = \frac{1}{2}\left({}_tu_{i,j}^{t+\Delta t} + {}_tu_{j,i}^{t+\Delta t} + {}_tu_{k,i}^{t+\Delta t}\, {}_tu_{k,j}^{t+\Delta t}\right) \tag{2.59} $$

where ${}_tu_{i,j}^{t+\Delta t}$ is the derivative of the displacement vector $\underline{u}^{t+\Delta t}$ at time $t+\Delta t$ with respect to the position vector at time t. For axisymmetric case, the strain component in θ-direction is given as

$$ {}_te_{\theta\theta}^{t+\Delta t} = \frac{u_r^{t+\Delta t}}{r^t} + \frac{1}{2}\left(\frac{u_r^{t+\Delta t}}{r^t}\right)^2 $$

An incremental decomposition of stress and strain gives

$$ \begin{aligned} {}_tS_{ij}^{t+\Delta t} &= {}_tS_{ij}^t + {}_t\Delta S_{ij} \\ &= \sigma_{ij}^t + {}_t\Delta S_{ij}, \end{aligned} \tag{2.60} $$

$$ \delta_t e_{ij}^{t+\Delta t} = \delta_t \Delta\epsilon_{ij} + \delta_t \Delta\eta_{ij}, \tag{2.61} $$

where,

$$ {}_t\Delta\epsilon_{ij} = \frac{1}{2}\left({}_t\Delta u_{i,j} + {}_t\Delta u_{j,i}\right) \tag{2.62} $$

$$ \left(\text{for axisymmetric case} \qquad {}_t\Delta\epsilon_{\theta\theta} = \frac{{}_t\Delta u_r}{r^t} \right) $$

and

$$ {}_t\Delta\eta_{ij} = \frac{1}{2}\left({}_t\Delta u_{k,i}\right)\left({}_t\Delta u_{k,j}\right). \tag{2.63} $$

$$\left(\text{for axisymmetric case} \qquad {}_t\Delta\eta_{\theta\theta} = \frac{1}{2}\left(\frac{{}_t\Delta u_r}{r^t}\right)^2 \right)$$

Here ${}_t\Delta u_{i,j}$ stands for the derivative of ${}_t\Delta\underline{u}$ (incremental displacement vector at time t) with respect to $\underline{r}^t$ (position vector at time t). Thus, eq. (2.57) with incremental decomposition can be written as

$$\int_{V^t} {}_t\Delta S_{ij}\delta({}_t\Delta\epsilon_{ij})\mathrm{d}V^t + \int_{V^t} {}_t\Delta S_{ij}\delta({}_t\Delta\eta_{ij})\mathrm{d}V^t + \int_{V^t} \sigma^t_{ij}\delta({}_t\Delta\eta_{ij})\mathrm{d}V^t + \int_{V^t} \sigma^t_{ij}\delta({}_t\Delta\epsilon_{ij})\mathrm{d}V^t = \bar{R}^{t+\Delta t}. \tag{2.64}$$

The 2nd integral on the left hand side is a higher order term compared to other terms and hence can be neglected. Moreover, using an elastic-plastic incremental stress-strain relationship (eq. 2.20), ${}_t\Delta S_{ij}$ can be approximated as ${}_tC^{EP}_{ijkl}\,{}_t\Delta\epsilon_{kl}$. Here, the left subscript of ${}_tC^{EP}_{ijkl}$ denotes the time at which it is to be evaluated. The above simplification will definitely give rise to an error in the right hand side of eq. (2.64). The error is normally neutralised by using some iterative scheme like Newton Raphson Method which is discussed in subsection 2.3.4. Now, eq. (2.64) can be written as

$$\int_{V^t} {}_tC^{EP}_{ijkl}{}_t\Delta\epsilon_{kl}\delta({}_t\Delta\epsilon_{ij})\mathrm{d}V^t + \int_{V^t} \sigma^t_{ij}\delta({}_t\Delta\eta_{ij})\mathrm{d}V^t + \int_{V^t} \sigma^t_{ij}\delta({}_t\Delta\epsilon_{ij})\mathrm{d}V^t = R^{t+\Delta t}. \tag{2.65}$$

Owing to the symmetries in ${}_tC^{EP}_{ijkl}$, ${}_t\Delta\epsilon_{ij}$, ${}_t\Delta\eta_{ij}$ and σ^t_{ij}, eq. (2.65) can be rewritten in the following form:

$$\int_{V^t} \left(\delta_t\{\Delta\epsilon\}^T\right) {}_t[C]^{EP}{}_t\{\Delta\epsilon\}\mathrm{d}V^t + \int_{V^t} \left(\delta_t\{\Delta\eta\}^T\right)[T]^t{}_t\{\Delta\eta\}\mathrm{d}V^t + \int_{V^t} \left(\delta_t\{\Delta\epsilon\}^T\right)\{\sigma\}^t\mathrm{d}V^t = R^{t+\Delta t}. \tag{2.66}$$

where,

$${}_t\{\Delta\epsilon\} = \{{}_t\Delta\epsilon_{rr},\ {}_t\Delta\epsilon_{zz},\ 2{}_t\Delta\epsilon_{rz},\ {}_t\Delta\epsilon_{\theta\theta}\}^T, \tag{2.67}$$

$$\{\sigma\}^t = \{\sigma^t_{rr},\ \sigma^t_{zz},\ \sigma^t_{rz},\ \sigma^t_{\theta\theta}\}^T, \tag{2.68}$$

$${}_t\{\Delta\eta\} = \{{}_t\Delta u_{r,r},\ {}_t\Delta u_{r,z},\ {}_t\Delta u_{z,r},\ {}_t\Delta u_{z,z},\ \frac{{}_t\Delta u_r}{r^t}\}^T, \tag{2.69}$$

$$[T]^t = \begin{bmatrix} [\Sigma]^t & 0 & 0 \\ 0 & [\Sigma]^t & 0 \\ 0 & 0 & [\Sigma]^t \end{bmatrix} \tag{2.70}$$

and

$$[\Sigma]^t = \begin{bmatrix} \sigma^t_{rr} & \sigma^t_{rz} & 0 \\ \sigma^t_{zr} & \sigma^t_{zz} & 0 \\ 0 & 0 & \sigma^t_{\theta\theta} \end{bmatrix} \tag{2.71}$$

The ${}_t[C]^{EP}$ matrix is the elastic-plastic matrix evaluated at time t which is given by eq. (2.53).

2.3.3 FEM Equations

The domain is discretised into a number of elements and the incremental displacement field over a typical element e is approximated as

$${}_t\{\Delta u\} = [Q]\,{}_t\{\Delta u\}^e \tag{2.72}$$

where,

$${}_t\{\Delta u\}^e = \{{}_t\Delta u^1_r,\ {}_t\Delta u^1_z, \ldots, {}_t\Delta u^n_r,\ {}_t\Delta u^n_z\}.$$

and ${}_t\Delta u^i_r$, ${}_t\Delta u^i_z$ stand for the (unknown) incremental displacements of node 'i' in r and z directions respectively . Here

$$[Q] = \begin{bmatrix} \{Q_1\}^T \\ \{Q_2\}^T \end{bmatrix} \tag{2.73}$$

where

$$\begin{aligned} \{Q_1\}^T &= \begin{bmatrix} N_1 & 0 & N_2 & 0 & \ldots & N_n & 0 \end{bmatrix}, \\ \{Q_2\}^T &= \begin{bmatrix} 0 & N_1 & 0 & N_2 & \ldots & 0 & N_n \end{bmatrix}. \end{aligned} \tag{2.74}$$

and N_i, the functions of (r, z), are called the *shape functions.*

With displacement field defined by eq. (2.72), the strain field within the element can be calculated in terms of nodal displacements. From eq. (2.72),

$${}_t\Delta u_{i,j} = \frac{\partial_t \Delta u_i}{\partial_t r_j} = {}_t\{Q_i\}^T_j\,{}_t\{\Delta u\}^e \tag{2.75}$$

where

$${}_t\{Q_i\}^T_j = \frac{\partial\{Q_i\}^T}{\partial_t r_j}. \tag{2.76}$$

Substituting eq. (2.75) in eqs. (2.62) and (2.63) and arranging them in vector form. we get the strain displacement relations:

$$ {}_t\{\Delta\epsilon\} = {}_t[B_L]\,{}_t\{\Delta u\}^e, \tag{2.77} $$

$$ {}_t\{\Delta\eta\} = {}_t[B_N]\,{}_t\{\Delta u\}^e \tag{2.78} $$

where,

$$ {}_t[B_L] = \begin{bmatrix} {}_t\{Q_1\}_{,r}^T \\ {}_t\{Q_2\}_{,z}^T \\ {}_t\{Q_2\}_{,r}^T + {}_t\{Q_1\}_{,z}^T \\ \frac{{}_t\{Q_1\}^T}{r^t} \end{bmatrix} \tag{2.79} $$

and

$$ {}_t[B_N]^T = \begin{bmatrix} {}_t\{Q_1\}_{,r}^T & {}_t\{Q_1\}_{,z}^T & {}_t\{Q_2\}_{,r}^T & {}_t\{Q_2\}_{,z}^T & \frac{{}_t\{Q_1\}^T}{r^t} \end{bmatrix} \tag{2.80} $$

Using the strain displacement relations derived above, the contribution to the integral (eq. 2.66) from a typical element e (with volume V_e^t) can be written as

$$ \begin{aligned} &\delta_t\{\Delta u\}^{eT} \left(\int_{V_e^t} {}_t[B_L]^T\, {}_t[C]^{EP}\, {}_t[B_L]\, \mathrm{d}V^t \right) {}_t\{\Delta u\}^e + \\ &\delta_t\{\Delta u\}^{eT} \left(\int_{V_e^t} {}_t[B_N]^T\, [T]^t\, {}_t[B_N]\, \mathrm{d}V^t \right) {}_t\{\Delta u\}^e + \\ &\delta_t\{\Delta u\}^{eT} \left(\int_{V_e^t} {}_t[B_L]^T\, \{\sigma\}^t\, \mathrm{d}V^t \right) = \delta_t\{\Delta u\}^{eT}\, ({}_{t+\Delta t}\{F\}^e) \end{aligned} \tag{2.81} $$

Here, the contribution to the term $R^{t+\Delta t}$ from the element e has been expressed in terms of the elemental external force vector ${}_{t+\Delta t}\{F\}^e$ using a standard procedure. Since the variation in the incremental displacement vector $\delta_t\{\delta u\}^e$ is arbitrary, expressing the term within Ist parenthesis as linear elemental stiffness $[\,K_L\,]^e$ and that of 2nd one as nonlinear elemental stiffness $[\,K_{NL}\,]^e$ the above equation can be written as

$$ ({}_t[K_L]^e + {}_t[K_{NL}]^e)\, {}_t\{\Delta u\}^e + {}_t\{f\}^e = {}_{t+\Delta t}\{F\}^e \tag{2.82} $$

or

$$ {}_t[K]^e\, {}_t\{\Delta u\}^e + {}_t\{f\}^e = {}_{t+\Delta t}\{F\}^e. \tag{2.83} $$

where

$$ {}_t\{f\}^e = \int_{V_e^t} {}_t[B_L]^T \{\sigma\}^t \, dV^t. \tag{2.84} $$

is the internal force vector.

Assembling the elemental matrices ${}_t[K]^e$ and the elemental vectors ${}_t\{f\}^e$ and ${}_{t+\Delta t}\{F\}^e$ over all the elements, we get the following global equation :

$$ {}_t[K]\,{}_t\{\Delta u\} + {}_t\{f\} = {}_{t+\Delta t}\{F\}. \tag{2.85} $$

Here ${}_t[K]$ is the global stiffness matrix, ${}_t\{\Delta u\}$ is the global incremental displacement vector (at time t) and ${}_t\{f\}$ and ${}_{t+\Delta t}\{F\}$ are the global internal and external force vectors respectively. Decomposing ${}_{t+\Delta t}\{F\}$, eq. (2.85) can be written as

$$ {}_t[K]\,{}_t\{\Delta u\} + {}_t\{f\} = {}_t\{F\} + {}_t\{\Delta F\}. \tag{2.86} $$

Here, ${}_t\{F\}$ is the (global) external force vector at time t and ${}_t\{\Delta F\}$ is the (global) incremental force vector from time t to $t + \Delta t$. In updated Lagrangian formulation, it is assumed that the equilibrium equations have been satisfied exactly at time t. Thus,

$$ {}_t\{f\} = {}_t\{F\}. \tag{2.87} $$

Then, eq. (2.86) reduces to

$$ {}_t[K]\,{}_t\{\Delta u\} = {}_t\{\Delta F\}. \tag{2.88} $$

Now, suppose we find the incremental stresses corresponding to the solution (${}_t\{\Delta u\}$) of eq. (2.88), add those to the earlier stresses to find the stresses at time $t + \Delta t$ and use eq. (2.84) to determine the internal force vector ${}_{t+\Delta t}\{f\}$ at time $t + \Delta t$, it is possible that it may not match with the applied (or external) force vector. Thus, eq. (2.88) represents only an approximate equilibrium equation at time $t + \Delta t$ (The approximation is mostly due to the linearization and simplification involved in the steps between eqs. 2.64 to 2.65). A solution of such an approximate equation may involve a significant amount of error and, depending on the time/load step, may becomes unstable. Therefore, it is necessary to modify eq. (2.88) to turn it into an iterative problem capable of providing a solution with desirable accuracy. The details of the iteration scheme is discussed in next section.

2.3.4 Numerical Scheme

The finite element equation of an elastic-plastic material (eq. 2.88) can be solved iteratively by various numerical schemes. Newton Raphson scheme is one of the most commonly used method for such problems. However, if the incremental load step is too large, the error involved in the computation of stress from the $[C]^{EP}$ matrix, evaluated at the previous point, also becomes large [30]. In such a situation, the backward return algorithm can be used to minimize the error. Another limitation of Newton Raphson method is that it often fails to converge in the neighborhood of critical point.

Normally we encounter two types of problems in mechanics: (1) Load control problem and (2) Displacement control problem. In a load control problem, the desired deformation is achieved by prescribing a load at a point. On the other hand, in a displacement control problem, it is the prescribed displacement which gives the desired deformation. In a load control problem, if the load falls due to change in geometry,then most iterative schemes fail to converge. Displacement control problems are free from this limitation. In this thesis, only displacement control problems are considered.

(I) The Newton Raphson Scheme

The scheme is best described with the help of Fig. (2.3) in the following steps. In Fig. (2.3), m is an equilibrium point at load level $\{P\}$. The aim is to reach another equilibrium point ($m+1$) at a load level ($\{P\}+\Delta\{P\}$).

Step 1 – First of all, the stiffness matrix ${}_t[K]$ in eq. (2.88) is evaluated using the stresses corresponding to point m. Next, eq. (2.88) is solved with ${}_t\{\Delta F\} = \{\Delta P\}$ to get an incremental displacement vector ${}_t\{\Delta u\}$.

Step 2 – From the incremental nodal displacements, incremental strain components are calculated by using eq. (2.77). Incremental stresses are calculated from the incremental strains by using suitable constitutive relation. Generally incremental stresses are calculated at the Gauss points of the elements. If the point under consideration is in elastic range, the elastic stress-strain matrix $[C]$ is used. Otherwise, elastic-plastic matrix $[C]^{EP}$ is used. Since elastic-plastic matrix is dependent on the current state of stress, the stress value at position m is used for the computation of

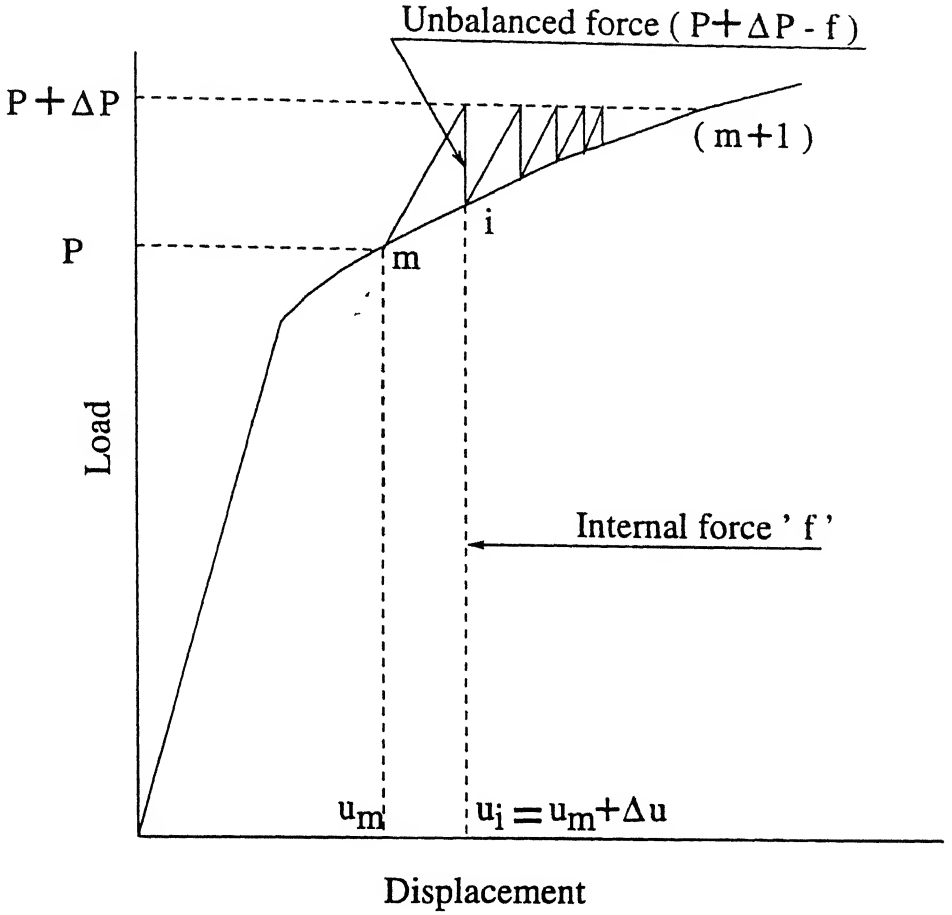

Figure 2.3: Illustration of Newton Raphson iterative scheme for a single load

elastic-plastic matrix. Eq. (2.23) is used to calculate Jaumann stress rate and the total Cauchy stress follows from eq. (2.24).

Step 3 – Once the stresses are calculated at all the Gauss points of all the elements, the internal nodal force vector ${}_{t+\Delta t}\{f\}$ is calculated. This force corresponds to the equilibrium load at point i in Fig. (2.3).

Step 4 – Since the applied nodal forces $({}_t\{P\} + {}_t\{\Delta P\}$ are not equal to internal nodal forces ${}_{t+\Delta t}\{f\}$, the deformed configuration is not an equilibrium configuration at load level $({}_t\{P\} + {}_t\{\Delta P\})$. It gives rise to an unbalanced nodal forces $({}_t\{P\} + {}_t\{\Delta P\} - {}_{t+\Delta t}\{f\})$.

Step 5 – The steps 1 to 3 are repeated with unbalanced nodal forces as the load vector and i as a starting point. Successive repetition of the above steps will lead to the equilibrium point $(m+1)$ for load level ${}_t\{P\} + {}_t\{\Delta P\}$ when the unbalanced nodal forces become almost zero(less than a preassigned quantity). In each successive iteration ,incremental displacement vector is added to its previous value.

Faster convergence is achieved if the tangential stiffness matrix at each successive equilibrium points is updated. The general practise is to achieve the total load in several increments. Within each incremental load step, Newton Raphson iterative scheme is applied with the same tangential stiffness matrix. Stiffness matrix is updated only when going for next load increment. This modified Newton Raphson scheme is a good compromise between reduced computational time and faster convergence.

(II) The Backward Return Algorithm

Consider the increment from point m to point i (See fig. 2.4). In calculation of the stresses at point i (in step 2 of the Newton Raphson scheme), we use the incremental stress-strain relation (eq. 2.37) where the $[C]^{EP}$ matrix is evaluated at point m. When the incremental load step is too large, this gives stresses not at point i but at some point i' which is not on the yield surface (see Fig. 2.4). Thus

$$\{\sigma\}_{i'} = \{\sigma\}_m + [C]_m^{EP}\{\Delta\epsilon\}. \tag{2.89}$$

A further return is required to bring the stresses to point i. Therefore we can write

$$\{\sigma\}_i = \{\sigma\}_{i'} + \{\Delta\sigma\}. \tag{2.90}$$

To determine $\{\Delta\sigma\}$, we proceed as follows. From eq. (2.50) and (2.53) we note that

$$[C]_m^{EP}\{\Delta\epsilon\} = [C]\{\Delta\epsilon\} - \mathrm{d}\lambda_m[C]\{a\}_m. \tag{2.91}$$

Therefore, to bring the stresses to point i, a correction is needed only in the second term. We assume that the correction can be approximated as

$$\{\Delta\sigma\} = -\mathrm{d}\lambda_o\,[C]\{a\}_{i'}. \tag{2.92}$$

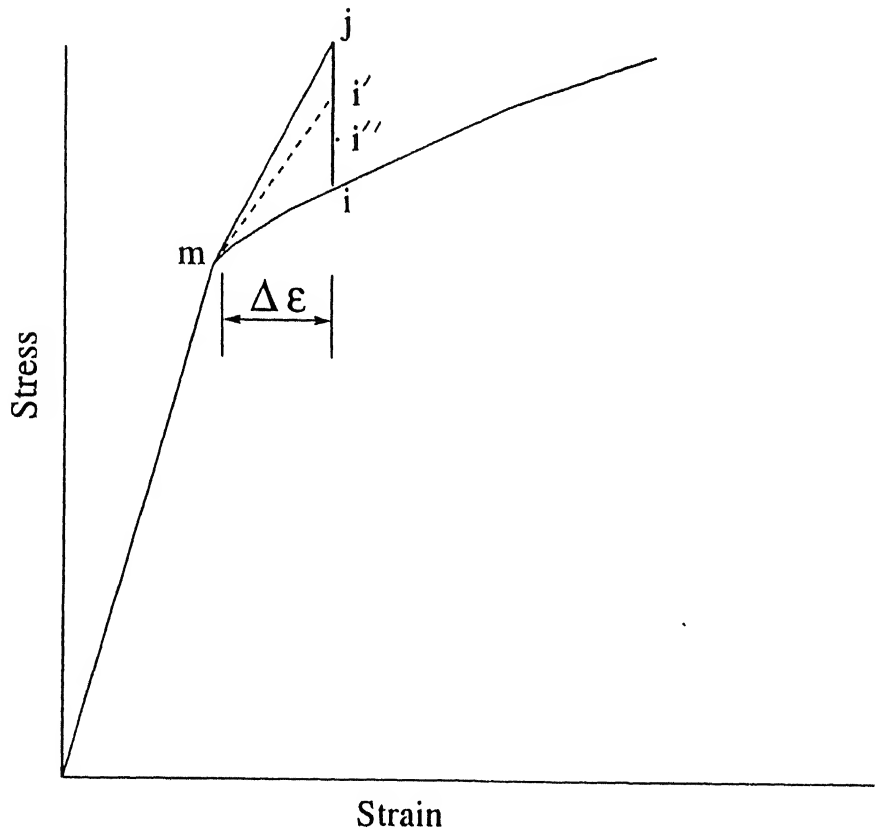

Figure 2.4: Illustration of Backward return algorithm

To determine the scalar $d\lambda_o$, we expand the plastic potential at point i'. Thus,

$$F_i = F_{i'} + \left(\frac{\partial F_{i'}}{\partial\{\sigma\}}\right)^T \{\Delta\sigma\} + \frac{\partial F_{i'}}{\partial p}\,\Delta p + \cdots \tag{2.93}$$

Analogous to eq. (2.45), we define $A_{i'}$ as

$$A_{i'} = -\frac{1}{d\lambda_o}\frac{\partial F_{i'}}{\partial p}\,\Delta p. \tag{2.94}$$

Substituting eq.s (2.92) and (2.94) in (2.93) and using the definition of flow vector $\{a\}_{i'}$ (eq. 2.44), we get

$$F_i = F_{i'} - d\lambda_o\,\{a\}_{i'}^T\,[C]\{a\}_{i'} - d\lambda_o\,A_{i'}. \tag{2.95}$$

Since the plastic potential has a zero value on the yield surface, $F_i = 0$. Thus

$$d\lambda_o = \frac{F_{i'}}{\{a\}_{i'}^T[C]\{a\}_{i'} + A_{i'}} \tag{2.96}$$

Substitution of eq.s (2.92) and (2.96) in (2.90) gives the following approximate expression for stress at point i:

$$\{\sigma\}_i \approx \{\sigma\}_{i'} - \frac{F_{i'}[C]\{a\}_{i'}}{\{a\}_{i'}^T[C]\{a\}_{i'} + A_{i'}}. \tag{2.97}$$

A further expansion will lead to the result

$$\{\sigma\}_i \approx \{\sigma\}_{i'} - \frac{F_{i'}[C]\{a\}_{i'}}{\{a\}_{i'}^T[C]\{a\}_{i'} + A_{i'}} - \frac{F_{i''}[C]\{a\}_{i''}}{\{a\}_{i''}^T[C]\{a\}_{i''} + A_{i''}} \cdots \tag{2.98}$$

where the point i'' is closer to point i than i' (see Fig. 2.4). When the plastic potential at point i becomes less than a pre assigned small number, no additional terms need to be added to equation (2.98).

2.4 Choice of Shape Functions and Numerical Integration

Since the finite element method is a numerical procedure for solving complex engineering problems, important considerations pertain to the convergence of the numerical solution. For monotonic convergence, the elements must be *complete* and the elements and mesh must be *compatible.* If these conditions are fulfilled, the accuracy of the solution increases continuously as we continue to refine the finite element mesh. This mesh refinement should be performed by subdividing a previously used element into two or more elements; thus, the old mesh must be " embedded " in the new mesh. *The requirement of completeness* of an element means that the polynomial approximating the displacements of the element must be able to represent the rigid body displacements and the constant strain fields. *The requirement of compatibility* means that the displacement within the element and across the element boundaries must be continuous.

Eq. (2.65) suggests that the convergence criterion will be satisfied if du_r and du_z are chosen to be bilinear functions of r and z. To satisfy the above condition, we have chosen the second order *Serendipity* approximation with eight noded rectangular elements for the finite element formulation. Here, the term r^2z^2 of the assumed approximation polynomial is omitted because it increases the size and the bandwidth of

the stiffness matrix without improving the approximation outside the element. The approximation is normally expressed in terms of the natural coordinates ξ and η. Thus, the shape functions N_i in eq. (2.74) are the second order *Serendipity shape functions* in ξ and η.

Exact evaluation of integrals appearing in element coefficient matrices and source vectors is not always possible because of the algebraic complexity of the coefficients in differential equations. In such cases, it is natural to seek numerical evaluation of these integral expression. Numerical evaluation of integrals, called numerical integration, involves approximation of the integrand by a polynomial of sufficient degree, because the integral of a polynomial can be evaluated exactly.

The most used numerical integration method is Gauss-Legendre numerical integration and formulae for integrals defined over a rectangular master element Ω_R is given by

$$\int_{\Omega_R} F(\xi,\eta)\,\mathrm{d}\xi\,\mathrm{d}\eta = \int_{-1}^{-1}\left[\int_{-1}^{-1} F(\xi,\eta)\,\mathrm{d}\eta\right]\mathrm{d}\xi \tag{2.99}$$

$$\approx \sum_{i=1}^{m}\sum_{i=1}^{n} F(\xi_i,\eta_j)\,w_i\,w_j \tag{2.100}$$

where m and n denote the number of quadrature points in the ξ and η directions, (ξ_i,η_j) denote the Gauss points, and w_i and w_j denote the corresponding Gauss weights.

2.5 Evaluation of the Secondary Variables

As explained above, solution of the problem is obtained in the form of nodal displacements. From nodal displacements, the secondary quantities like the upsetting load, the normal stress distribution at the tool-workpiece interface, the contours equivalent stress and strain and the deformed mesh are calculated. The details of these calculations are explained briefly in the following lines-

i. Upsetting Load :

Since complete sticking is assumed at the die-workpiece interface, there is no frictional loss at the interface. Then the supplied energy is exactly equal to the work

spent in creating the internal deformation. Thus, over the increment from t to $t+\Delta t$

$$({}_t\Delta F_z)\,({}_t\Delta u_z) = \int_{V^{t+\Delta t}} \sigma_{eq}^{t+\Delta t}\, {}_t\Delta\epsilon_{eq}\; 2\pi\, r^{t+\Delta t}\, \mathrm{d}r^{t+\Delta t}\, \mathrm{d}z^{t+\Delta t} \tag{2.101}$$

where ${}_t\Delta u_z$ = specified platen displacement in the increment

${}_t\Delta F_z$ = required incremental upsetting load

$$\sigma_{eq}^{t+\Delta t} = \left(\frac{3}{2}\sigma_{ij}^{\prime t+\Delta t}\,\sigma_{ij}^{\prime t+\Delta t}\right)^{\frac{1}{2}}, \tag{2.102}$$

= equivalent stress based on stress tensor at time $t+\delta t$

$${}_t\Delta\epsilon_{eq} = \left(\frac{2}{3}{}_t\Delta\epsilon_{ij}\,{}_t\Delta\epsilon_{ij}\right)^{\frac{1}{2}}, \tag{2.103}$$

= incremental equivalent strain from t to $t+\Delta t$

The incremental upsetting load is found from eq. (2.101).

ii. Surface Contact Stress Distribution :

The surface contact stress distribution is evaluated by considering each of the billet elements in contact with the platen and by linearly extrapolating from the values of σ_{zz} at the Guass points.

iii. Equivalent Stress and Strain :

The equivalent stress (σ_{eq}) and the equivalent strain (ϵ_{eq}) are calculated at each Guass point from the components of stress and incremental strain tensors at that Guass point by using eq. s(2.102) and (2.103) and the following relation :

$$\epsilon_{eq}^{t+\Delta} = \sum^{t+\Delta t} \Delta\epsilon_{eq}$$

Then, the contours of σ_{eq} and ϵ_{eq} are plotted using the values evaluated at 2x2 Guass points of the elements.

iv. Deformed Mesh :

The deformed mesh of the workpiece is plotted to exhibit the deformation pattern. The deformed mesh after any increment can be obtained by updating the r and z coordinates of nodal points by using the displacement components upto that increment.

Chapter 3

Results And Discussion

The finite element modelling of an axisymmetric upsetting process developed in the previous chapter has been applied to a number of cases involving two metals and various sets of input variables to illustrate its applicability. The metals considered are aluminium 1100F and steel AISI 1019 whose material properties are given as below. The properties for the aluminium are taken from [21] and that of the steel from [23].

Material properties :
Aluminium 1100F

Young's modulus $E = 69{:}11\,\text{GPa}$

Poisson's ratio $\nu = 0{:}33$

Intial yield stress $Y_o = 89{:}85\,\text{MPa}$

Slope of effective stress and plastic strain curve $H' = 138{:}23\,\text{MPa}$

Steel AISI 1019

Young's modulus $E = 210\,\text{GPa}$

Poisson's ratio $\nu = 0{:}3$

Intial yield stress $Y_o = 478{:}2\,\text{MPa}$

Hardening parameter $K = 563{:}98\,\text{MPa}$

Hardening exponent $n = 0{:}14$

In this chapter, first a convergence study is performed to check the convergence of the finite element formulation with respect to the mesh size. Then, the finite element code is validated by comparing the results with the FEM and experimental results obtained by Lee and Kobayashi [21]. In the last section, the parametric study is carried out to illustrate the effects of various process variables on the process parameters.

3.1 Convergence Study

The convergence study is performed for the problem of an axisymmetric upsetting of an aluminium 1100 F cylinder with the height to diameter ratio of 1. 2. As stated in chapter 2, only a quadrant is chosen for the analysis. Initially, the mesh of 35-eight noded rectangular elements is selected (fig. 3.1). The elements along the die contact interface, along the free surface and along the axis of symmetry are made smaller as

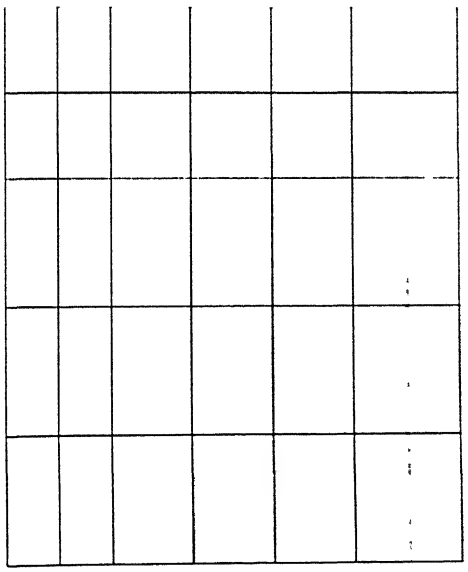

Figure 3.1: Coarse mesh (35 elements)

the stress/displacement gradients are likely to be high in these regions. Then, the refinement is performed by dividing each element into four elements forming a mesh of 140 elements. The results are obtained for both the meshes.

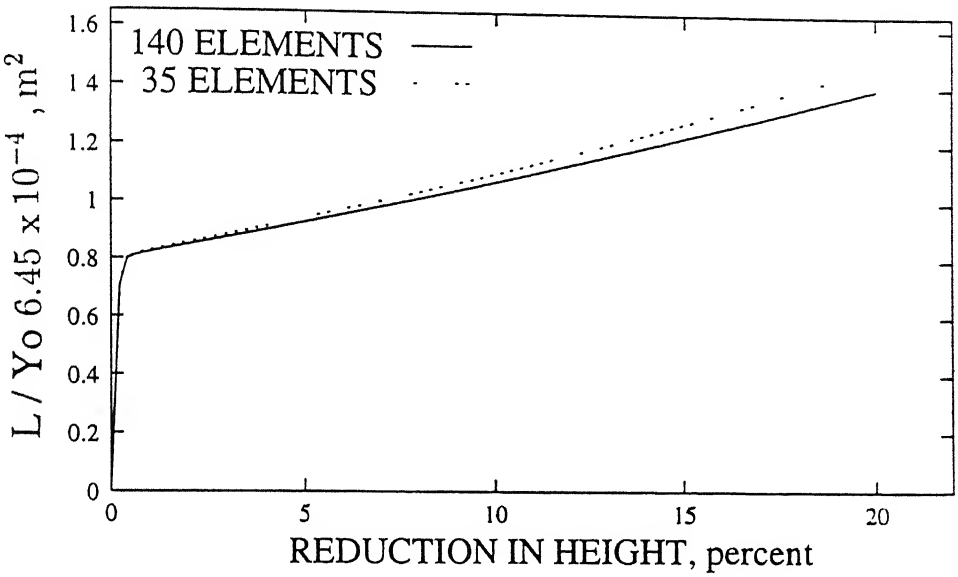

Figure 3.2: Convergence of load-displacement curve.

Fig. (3.2) shows the variation of non-dimensional load (the ratio of the upsetting load (L) to the initial yield strength of the metal) with percent reduction in height for the two cases. It can be seen from the figure that as we refine the mesh, the solution seems to converge. There is a decrease of 8.89 % in the load at 20 % reduction when the mesh is changed from the coarse mesh to the fine. It is also found during this study that a smaller increment of die displacement resulted in a slightly lower value of the upsetting load. Thus, the solution seems to converge as the sizes of both the elements and the displacement increment are reduced.

Fig. (3.3) shows the convergence of the bulge profile, i. e. the displacement of the free surface of the cylinder at 20 % reduction in height for the two meshes.

Figures (3.4a) and (3.4b) show the contours of equivalent strain at 20 % reduction in height for 35 elements and 140 elements respectively. It is found that the values of equivalent strain also have converged.

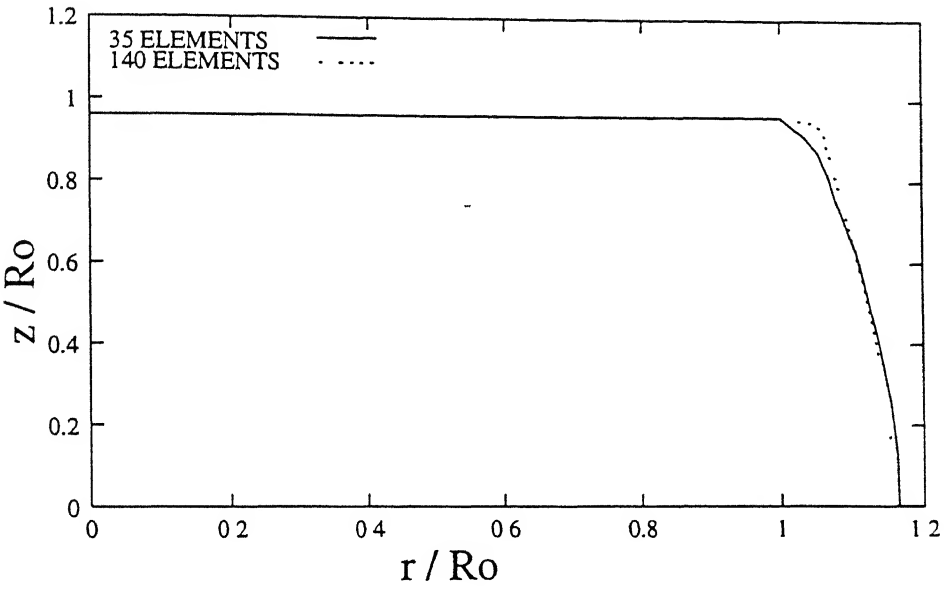

Figure 3.3: Convergence of bulge profile at 20 percent reduction in height.

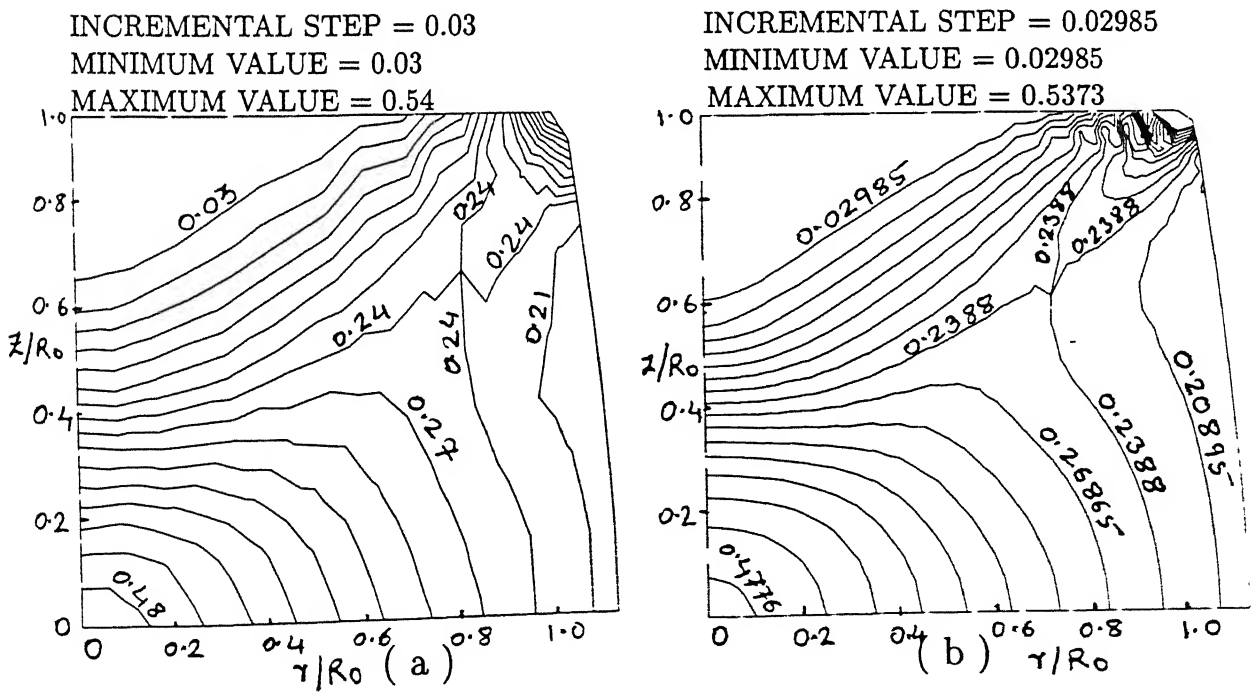

Figure 3.4: Convergence of contours of effective strain at 20% reduction in height

3.2 Validation

The computer code is validated by comparing the results with the FEM and experimental results of Lee and Kobayashi [21]. They performed the analysis of an axisymmetric upsetting process with the height to diameter ratio of 0.8 using a mesh of 124 four noded quadrilateral elements for half the cylindrical specimen. The material properties of Al 1100F were used for the analysis which was carried out upto a 33 percent reduction in height. The full sticking condition was used at the die-workpiece interface.

The same problem is solved using the developed finite element code. A quarter of the cylinder specimen is analysed using the mesh of 140 eight noded rectangular elements with smaller size elements along the die contact area, along the free surface and along the axis of symmetry.

Fig. (3.5) shows the comparison of the FEM and experimental load-displacement curves. The discrepancy between the theoretical and experimental predictions can

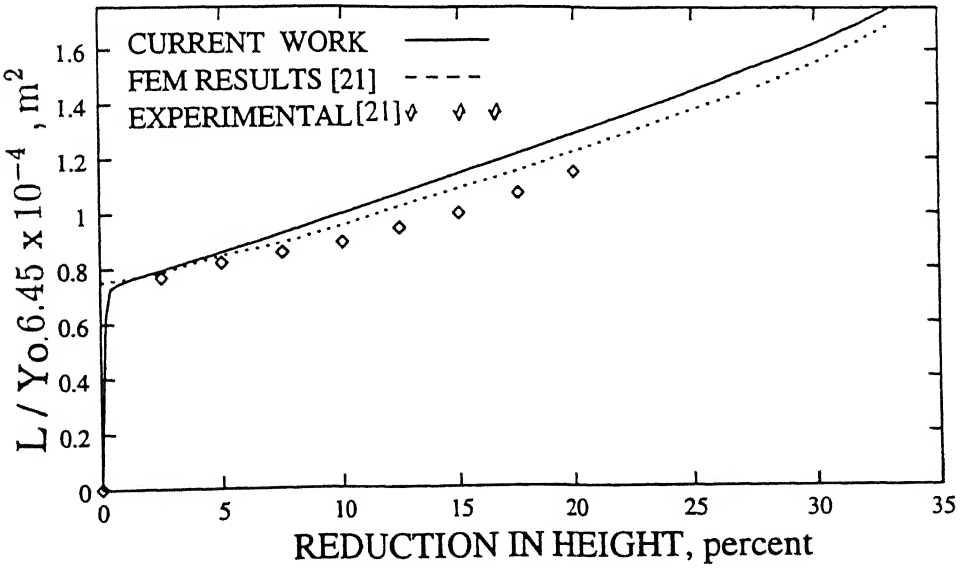

Figure 3.5: Comparison of theoretical and experimental load-displacement curves.

be explained as follows. In experimental studies, slip is observed over a part of the interface [21]. Whereas in theoretical modelling, full sticking is assumed over the whole interface. As a result, the theoretically predicted behaviour of the elements on the free

surface near the edge shows that they undergo a very large deformation (see figures 3.6a and 3.7a), which doesn't happen in real life upsetting process. Consequently, the theoretical predicted values of contact stress (near the edge of free surface) become very high as shown in fig. (3.9). Even though the theoretical model neglect the interfacial slip, the energy needed to create the above mentioned large deformation of the free surface elements seem to be more than what is dissipated due to the interfacial slip. This is the reason why the theoretically predicted values of the upsetting load are higher than the experimental values. The values of Lee and Kobayashi [21] are lower than the values predicted by the present study. This is because the deformation gets under-predicted (see fig. 3.7b) by the method of Lee and Kobayashi as they used the linearised incremental equations.

This phenomenon of very large deformation of the free surface corner elements is observed when H/D < 1 or %r > 20. Therefore, these cases are avoided in most of the parametric study carried out in section 3.3.

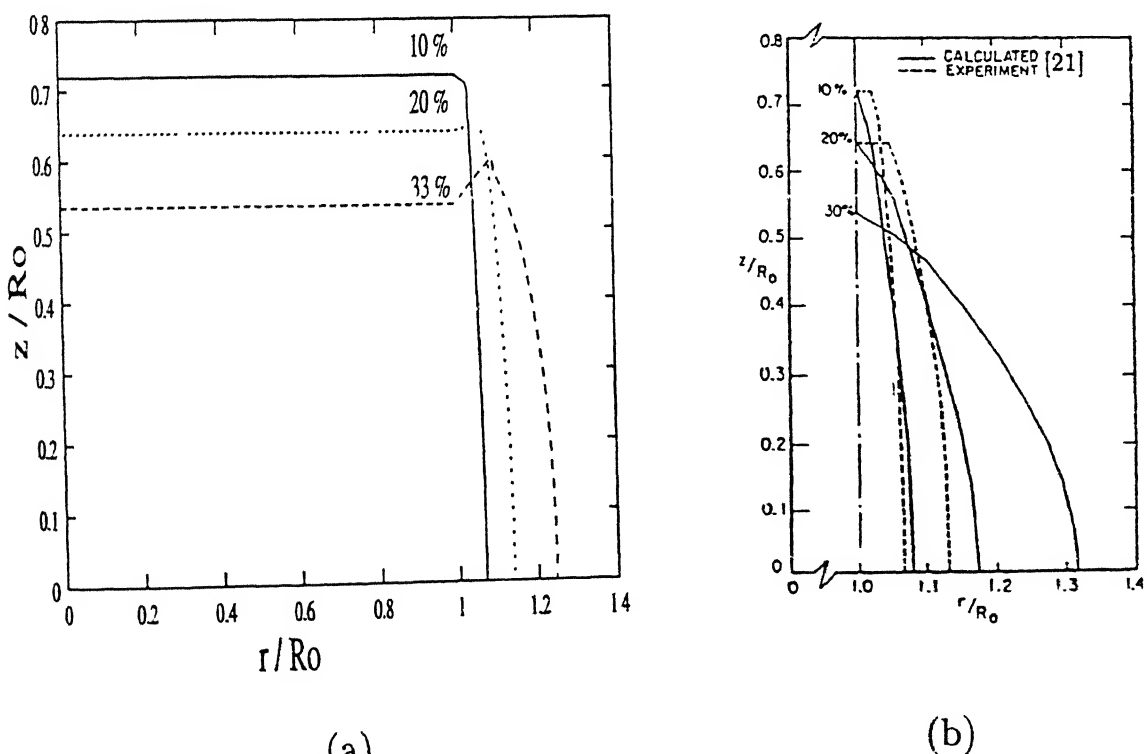

(a) (b)

Figure 3.6: Bulge profiles at various reductions in height.

Figures (3.6a) and (3.6b) show the comparison of the bulge profiles at various

reductions in height. For small reductions the theory well predicts the geometrical change of the free surface. The predictions, however, deviate from the observation as the reduction in height increases. After some stage of compression, the phenomenon of free-surface fold-over is predicted at the corners. The extent of this relative upward metal flow at the corners increases with friction and with the amount of deformation. In real upsetting, flow past the dies is not possible. Therefore, the originally free surface comes into contact with the die at the corners [31].

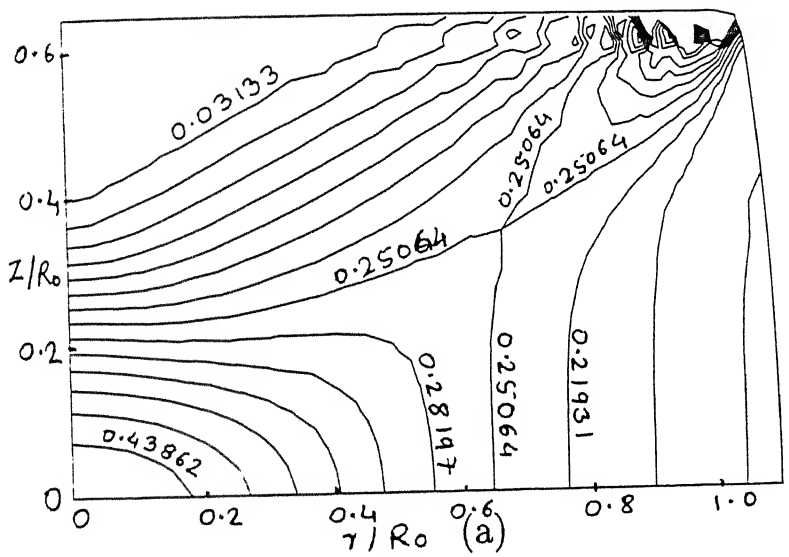

INCREMENTAL STEP = 0.03133

MINIMUM VALUE = 0.03133

MAXIMUM VALUE = 0.46995

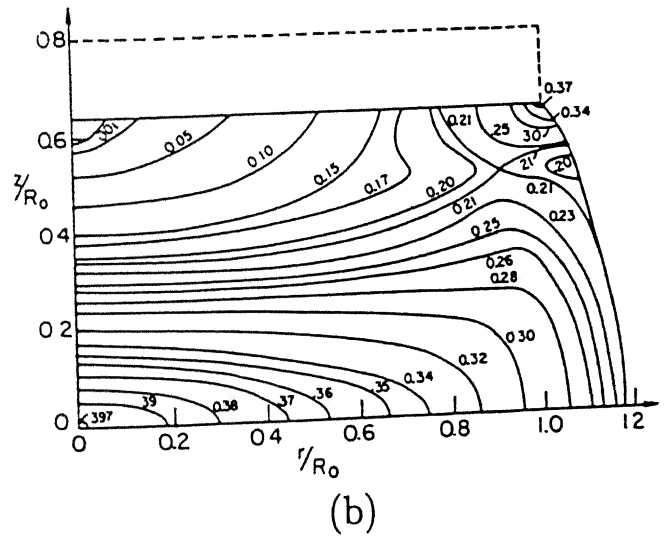

Figure 3.7: Distribution of effective strain at 20 percent reduction in height (a) present study (b) results of [21].

The effective strain is an indication of the degree of deformation, and can be calculated by following the deformation at any point incrementally. The comparison of the effective strain distributions at a 20 percent reduction is shown in fig. (3.7a) and 3.7b). A percentage error of 11.2 is observed with respect to the values of Lee and Kobayashi [21].

3.3 Parametric Study

In this section, a study is made of the effect of process variables viz. the percent reduction in height (%r), the height to diameter ratio (H/D) and the material properties on the important design parameters like the upsetting load, the contact pressure distribution at the interface, the bulge profile and the distributions of effective strain and effective stress.

3.3.1 Effects of Percent Reduction in Height and Height to Diameter Ratio

In this section, analysis is carried out for three cases of height to diameter ratio of cylindrical specimen (H/D = 1, 1.25 and 1.5) and for various values of percentage reduction from 5 to 20 percents. The material properties of aluminium 1100F are used.

1. **The Upsetting Load**

   Fig. (3.8) shows the relation between the upsetting load and the percentage reduction in height (i. e. the die displacement). The relation is linear in the elastic range as well as in the early stage of yielding, but it deviates after the plastic region spreads considerably. The upsetting load increases with reduction in height. Besides, as the figure indicates it decreases with H/D ratio. In real materials in which stress-strain curves are not straight but always convex to the upper direction, the load decreases with H/D ratio [32].

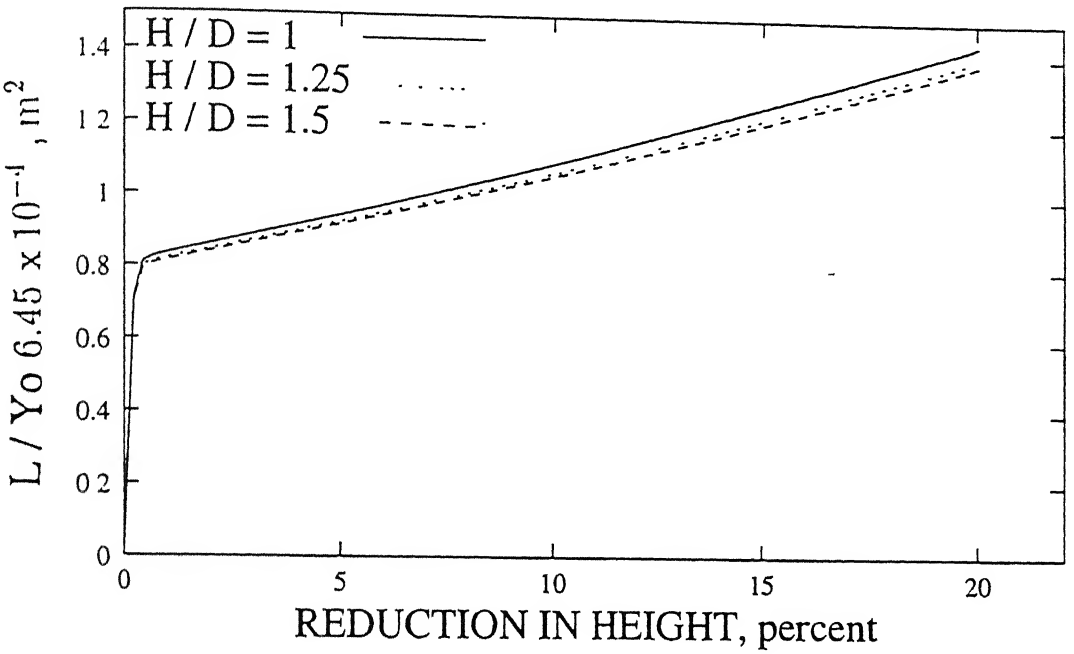

Figure 3.8: Load-displacement curves for various H/D ratios.

2. **Distribution of Contact Pressure on the Interface**

   Figures (3.9a and 3.9b) depict the distributions of normal contact stress on the interface of die and workpiece at 5 and 20 percent reductions in height respectively at three different values of H/D namely 1, 1.25, 1.5. The normal stress values increase with radius, r and tend to infinity at the edge $r = R_o$. This happens because of the assumption of full sticking condition. Similar trend is reported by Lee and Kobayashi [21]. If the interfacial slip is taken into account, the normal stress value is likely to be finite at the edge.

   The normal stress distribution doesn't change either with H/D or with percent reduction. However, the values increase with percent reduction (for the same H/D ratio) and decrease with H/D ratio (for the same percent reduction).

3. **Bulge Profile**

   Figures (3.10a and 3.10b) show the bulge profiles at 5 and 20 percent reductions respectively at three values of H/D (H/D=1, 1.25 and 1.5). Figures indicate that as upsetting advances, the bulge becomes larger. It is because the elements near the edge, which yield early suffer a large deformation with the increase in

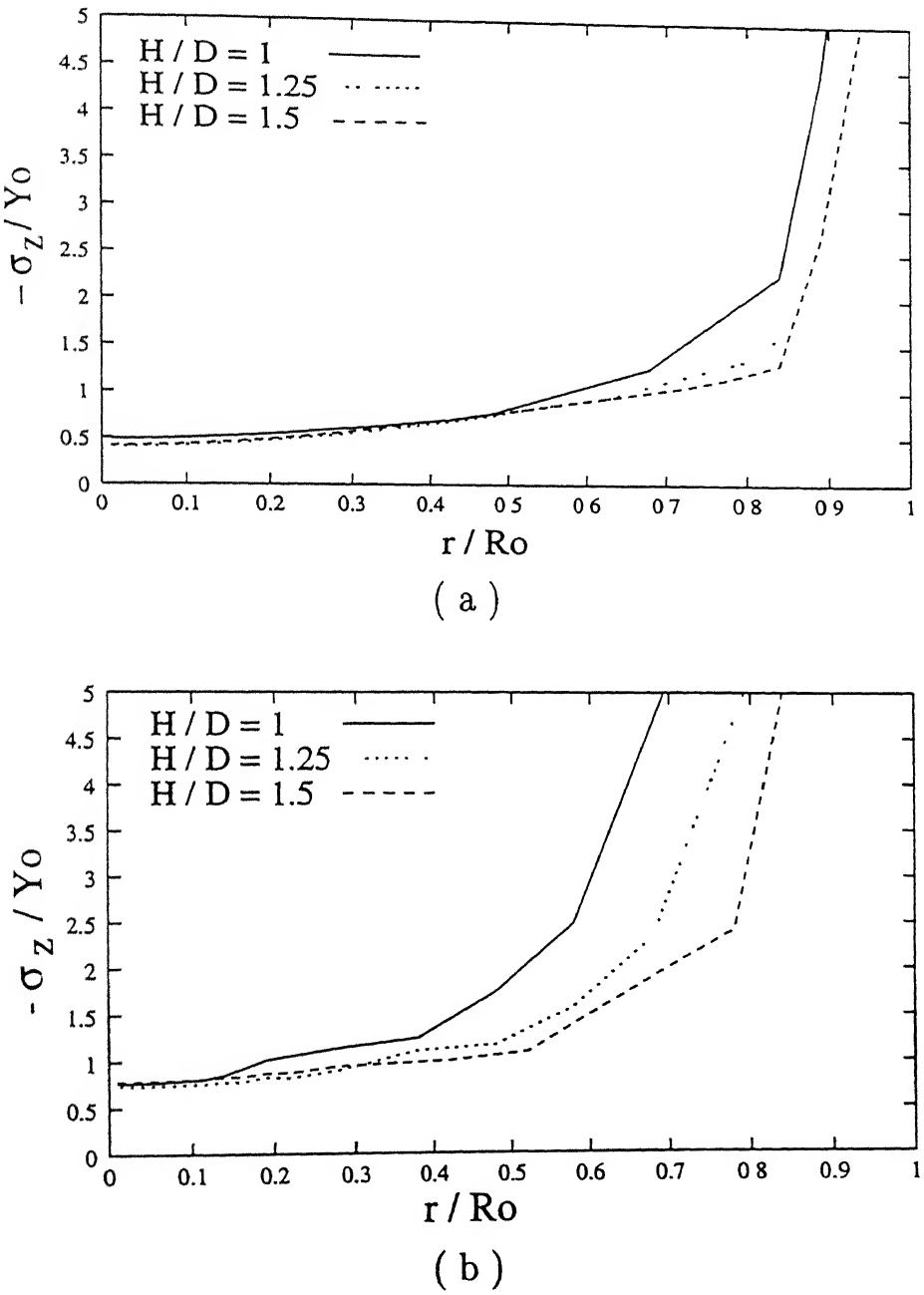

Figure 3.9: Distribution of normal contact stress at interface for various H/D ratios at (a) 5 percent reduction (b) 20 percent reduction.

reduction and the growth of bulge depends mainly on the deformation of these elements. At the same percentage reduction in height, the size of bulge increases in proportion to the H/D ratio.

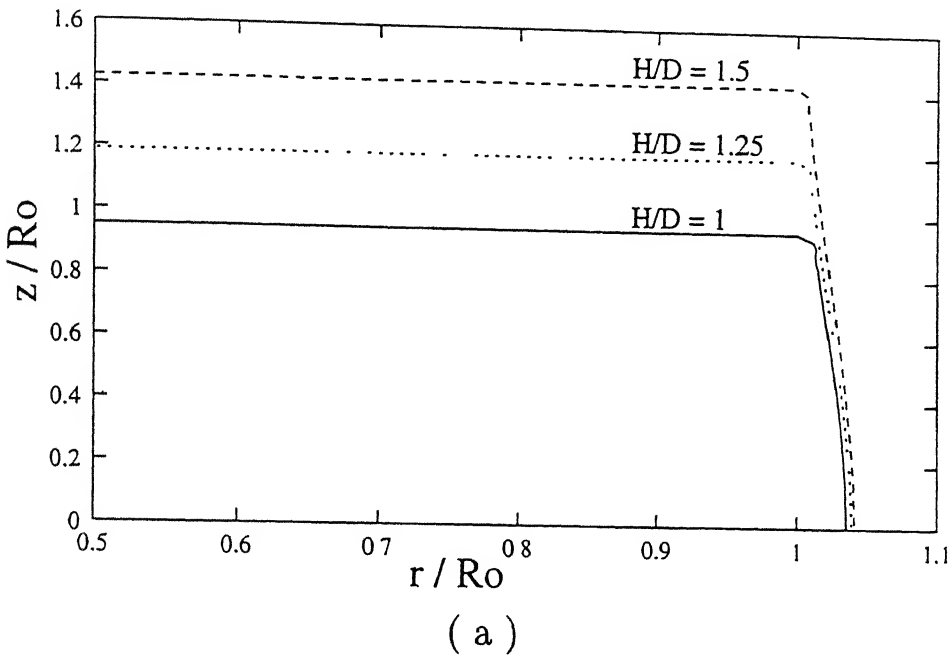

(a)

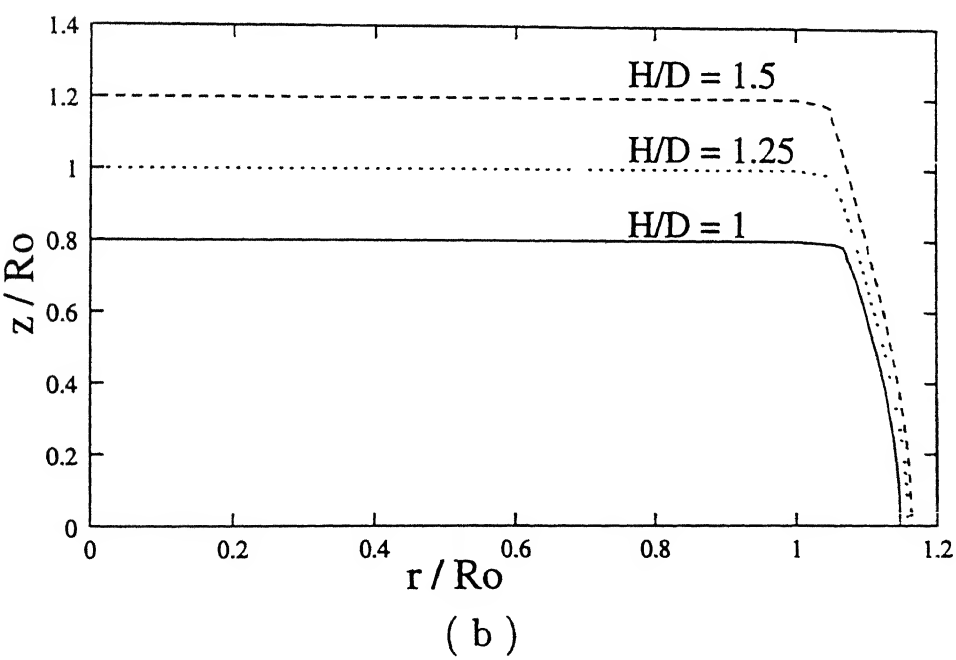

(b)

Figure 3.10: Bulge profiles of free surface for various H/D ratios at (a) 5 percent reduction (b) 20 percent reduction.

4. **Distribution of Effective Strain**

Figures (3.11a), (3.11b) and (3.11c) show the contours of effective strain for the following three cases respectively : (a) %r = 20, H/D = 1, (b) %r = 20, H/D = 1.5 and (c) %r = 33, H/D = 1. There is no significant change in the distribution pattern of effective strain when either %r or H/D is changed. However, the values

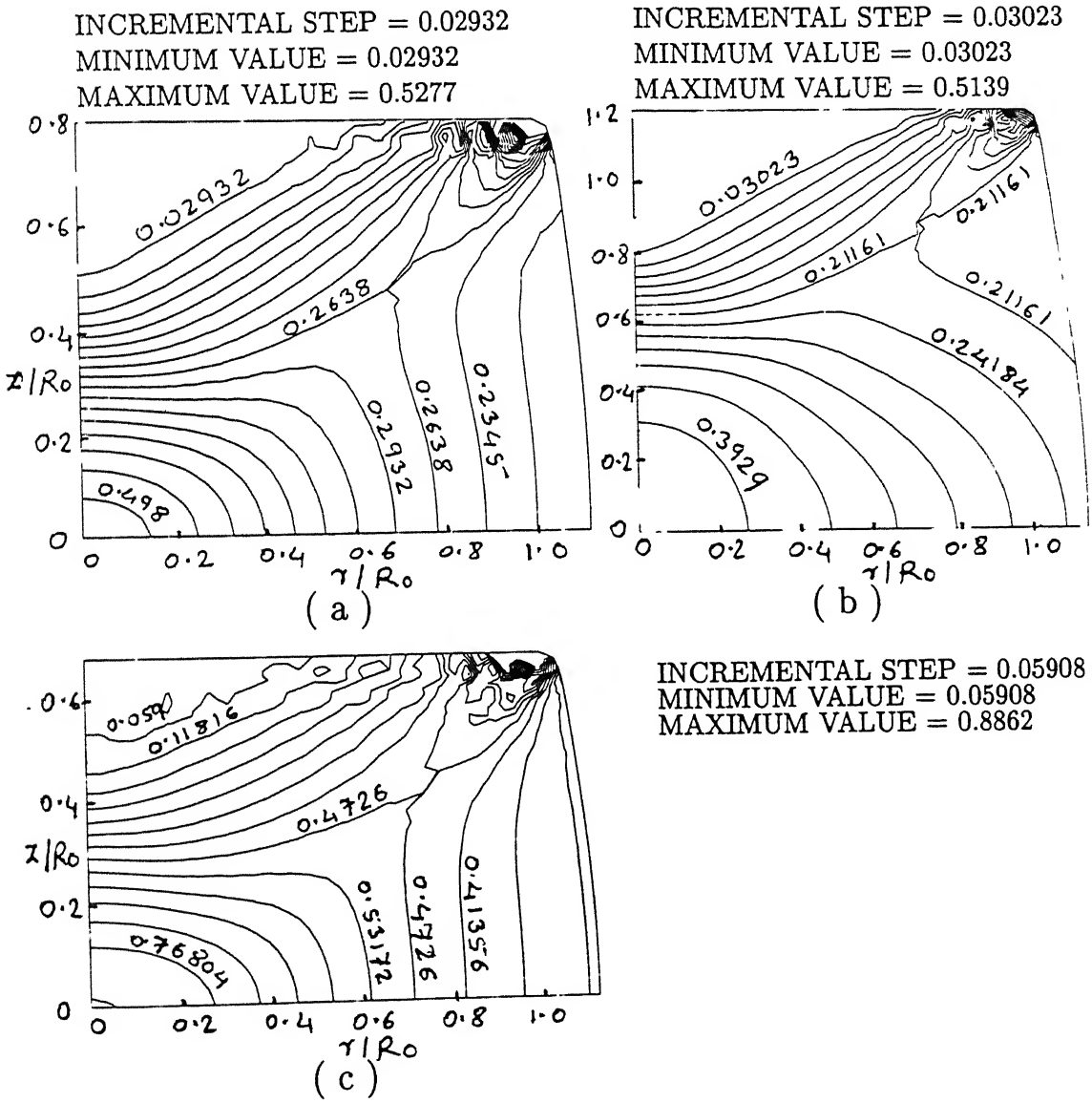

Figure 3.11: Contours of effective strain (a) %r = 20, H/D = 1 (b) %r = 20, H/D = 1.5 and (c) %r = 33, H/D = 1.

of effective strain decrease with H/D ratio and increase with %r.

5. **Distribution of Effective Stress**

Figures (3.12a), (3.12b) and (3.12c) show the contours of effective stress for the following three cases respectively : (a) %r =20,H/D = 1, (b) %r = 20, H/D = 1.5 and (c) %r = 33, H/D = 1.

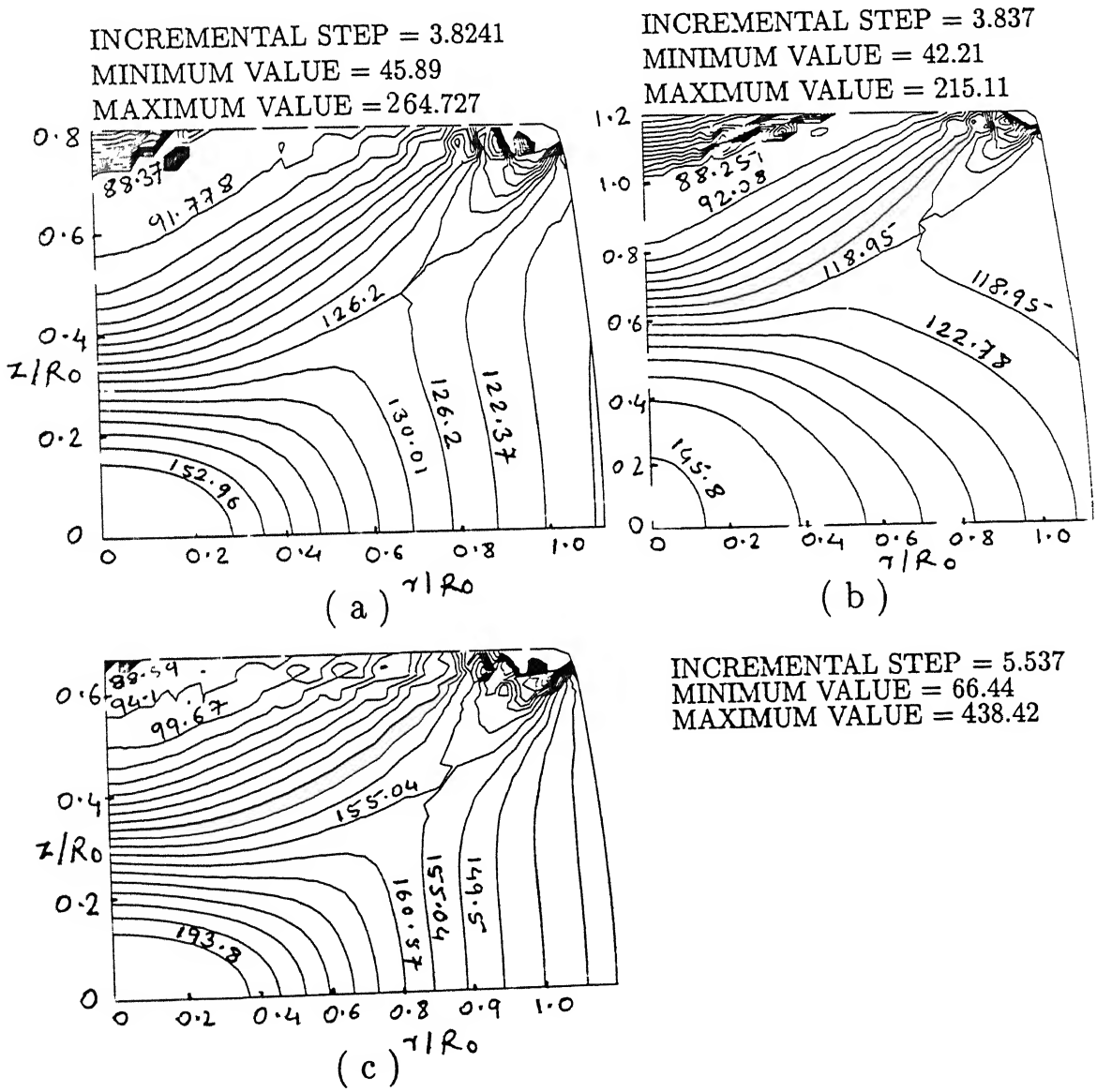

Figure 3.12: Contours of effective stress (a) %r = 20. H/D = 1 (b) %r = 20, H/D = 1.5 and (c) %r = 33, H/D = 1.

In the early stages of upsetting, the regions at the center and at the edge of the die-workpiece interface yield first ($\sigma_{eq} > 89{:}85$ MPa). As upsetting advances, these

regions spread and join each other. The figures show that, at 20% reduction, the region at the center of the interface has still not yielded. A small region near the free surface also has low values of equivalent stress as this region is un-restrained. At 33% reduction, the whole region becomes plastic.

The figures show that as H/D is increased, the values of effective stress decrease and the distribution pattern also changes.

6. **Deformed Mesh**

Figures (3.13a), (3.13b) and (3.13c) show the deformed mesh for the following cases : (a) %r = 20, H/D = 1, (b) %r = 20, H/D = 1.5 and (c) %r = 33, H/D

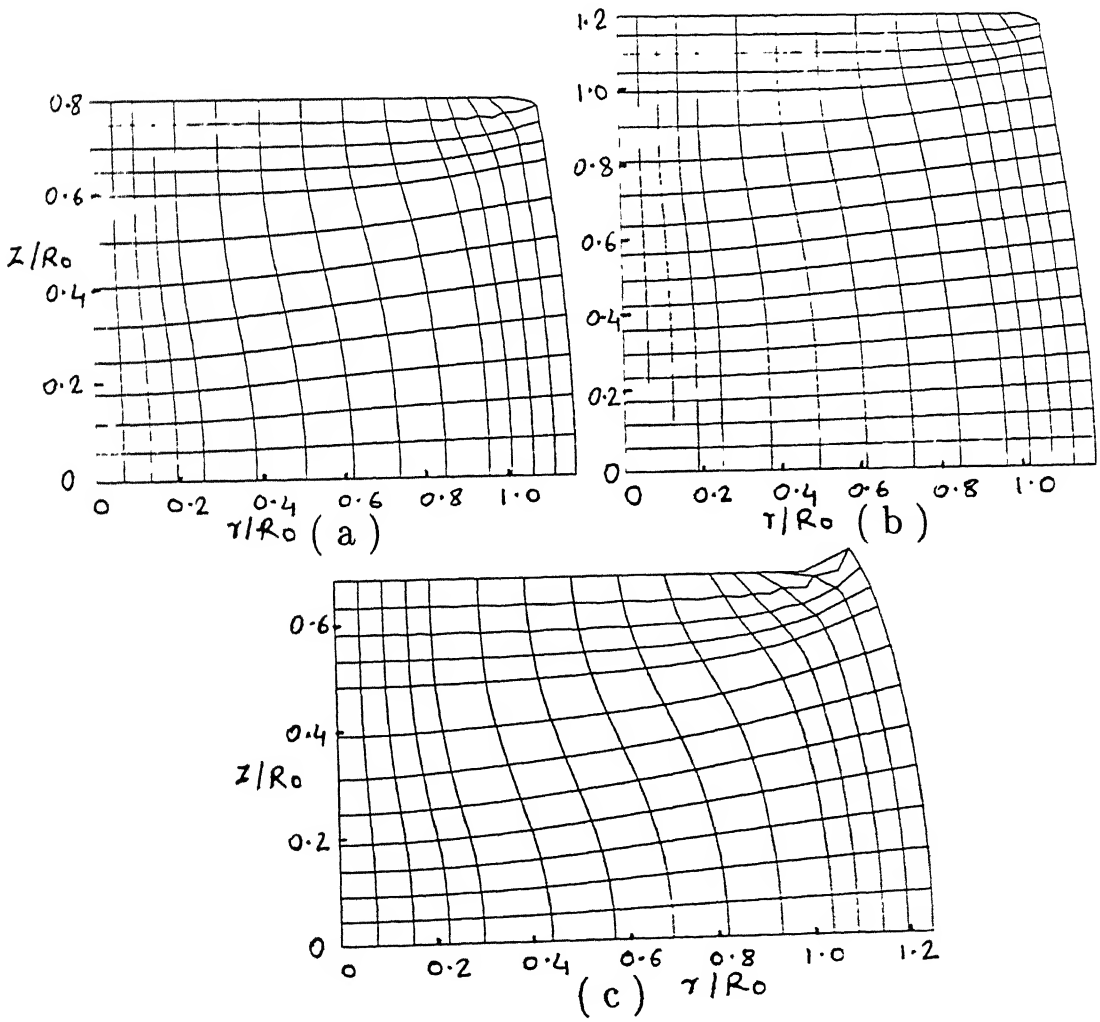

Figure 3.13: Deformed mesh (a) %r = 20, H/D = 1 (b) %r = 20, H/D = 1.5 and (c) %r = 33, H/D = 1.

= 1. The specimen with H/D ratio of 1.5 undergoes more deformation than that of H/D=1. Further, it is observed that upto 20% reduction in height, the phenomenon of free-surface fold-over doesn't appear as long as H/D ratio is larger than 1. However, whenever %r increases beyond 20 or H/D becomes less than 1. the fold-over of the free surface occurs as shown in fig. (3.13c).

3.3.2 Effect of Strain Hardening

In this section, the process parameters are obtained for two different materials namely aluminium 1100F and steel AISI 1019 to study the effect of strain hardening on them.

1. **The Upsetting Load**

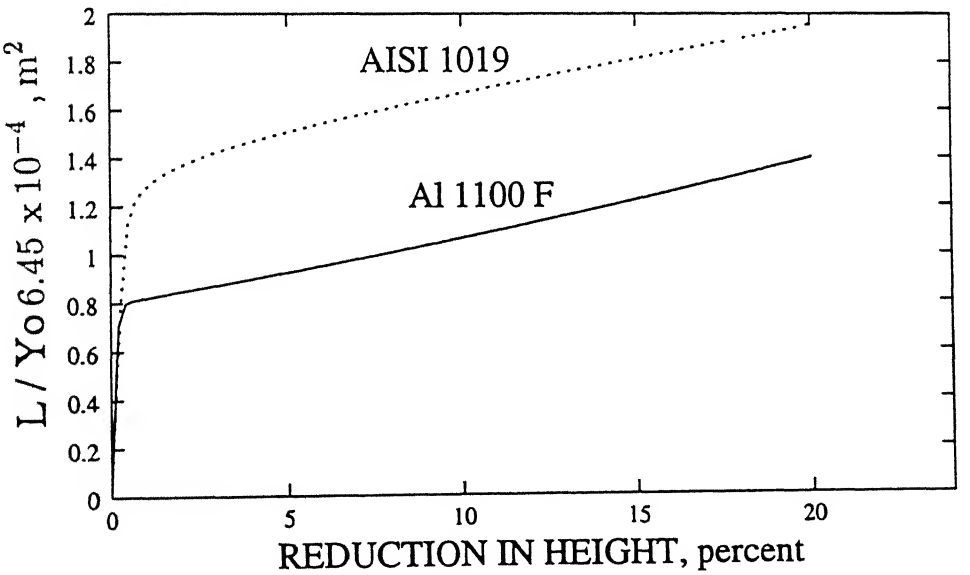

Figure 3.14: Load-displacement curves for aluminium and steel (H/D = 1.25)

Fig. (3.14) gives the comparison of load-displacement curves for steel and aluminium. The upsetting load required to deform the steel specimen is obviously larger than the one required for the aluminium specimen as the yield stress is larger. However, the load-displacement curves are similar even though the hardening laws are different.

2. **Distribution of Normal Contact Stress at the Interface**

Distribution of normal contact stress at tool-workpiece interface for the two metals is shown in fig. (3.15). The normal stress for steel is larger than the one for aluminium over the whole contact surface. This again is due to the larger values of the yield stress of steel. There is not much change in the contact stress distribution pattern of the two metals.

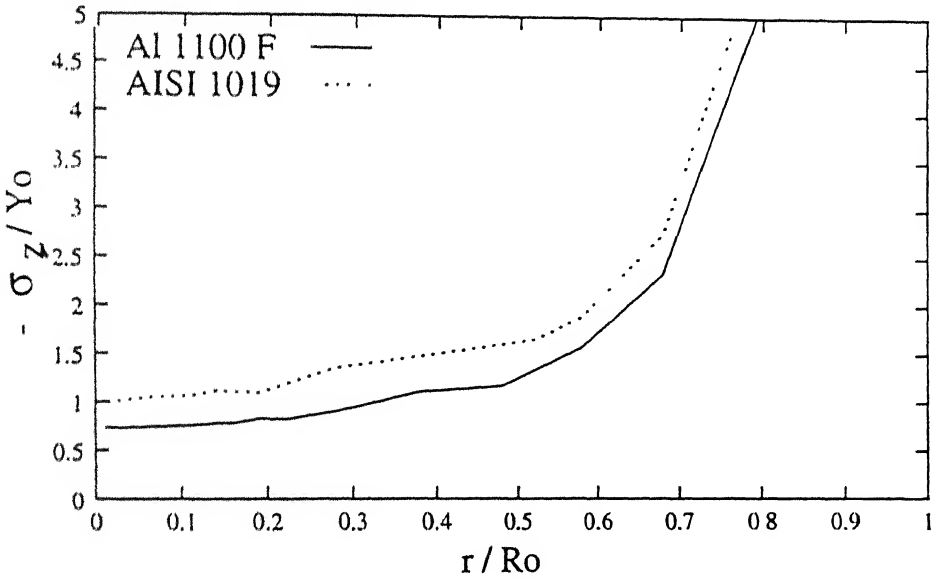

Figure 3.15: Distribution of normal contact stress at interface for two metals (%r = 20, H/D = 1.25)

3. **Bulge Profile**

Fig. (3.16) shows the bulge profiles of steel and aluminium specimens at 20 percent reduction in height and for H/D = 1.25. It is observed that bulge profiles are more or less the same. This shows that the bulge profile depends purely on the kinematic parameters like %r and H/D ratio and not an strain-hardening.

4. **Distribution of Effective Strain and Effective stress**

Fig. (3.17) shows the distributions of effective strain for aluminium and steel while fig. (3.18) shows the contours of effective stress for the two metals. The figure show that the pattern and the values of the effective strain are almost

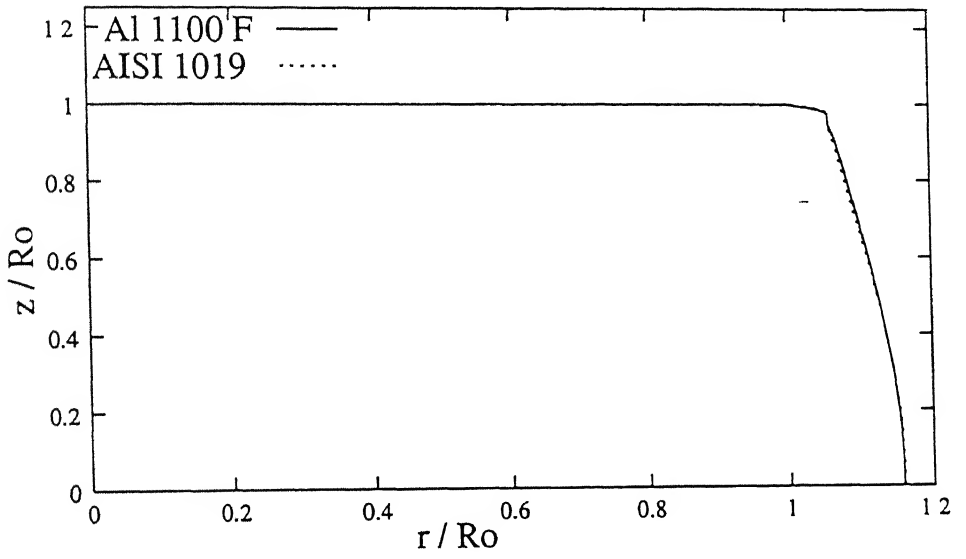

Figure 3.16: Bulge profiles of free surfaces for two metals (%r = 20, H/D = 1.25)

the same for the two metals. This implies that the effective strain distribution, like bulge profile, depends only on the kinematic parameters. The distribution patterns of the effective stress are also similar. The values for the steel specimen are of course larger.

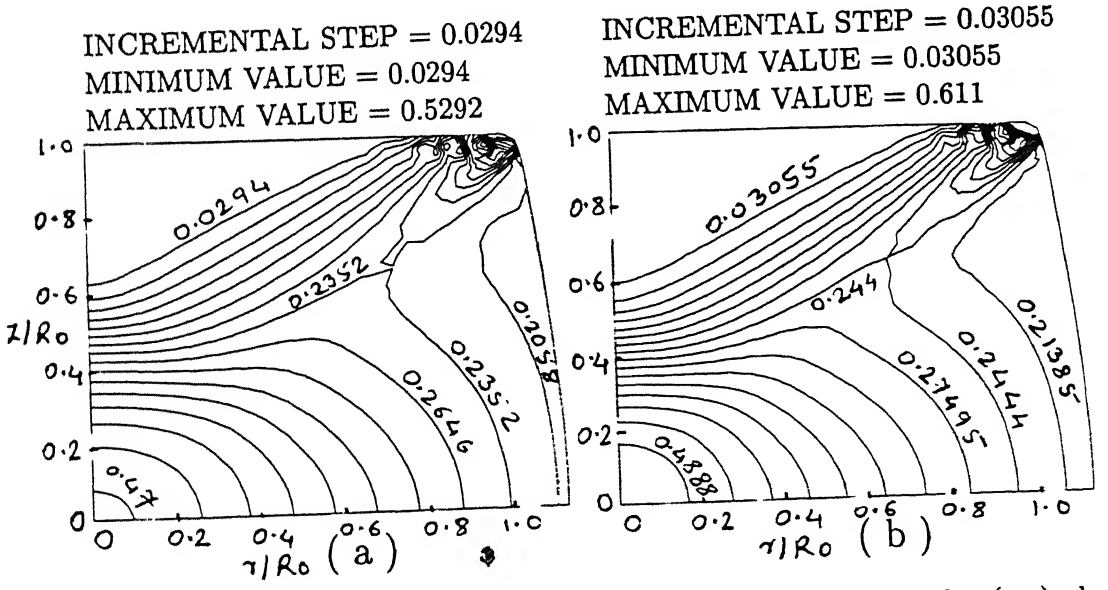

Figure 3.17: Contours of effective strain at 20%r and H/D = 1.25 for (a) aluminium and (b) steel.

Chapter 4

Summary, Conclusions and Scope for Further Work

In the present work, the axisymmetric upsetting problem under the condition of full sticking at the die-workpiece interface is solved by the finite element method considering the material to be elastic-plastic strain hardening yielding according to von Mises criterion. The inertial terms are neglected. The updated Lagrangian formulation which is convenient for handling material and geometric nonlinearities is used. The modified Newton- Raphson iterative scheme is used for solving the incremental equations. Since the method permits to follow the deformation in step-by-step manner, it is possible to determine the quantities at any instant. The usefulness of the method for carrying out detailed studies of the deformation and stress distributions in plasticity problems has been demonstrated.

The detailed parametric study has been carried out choosing aluminium as a material to manifest the effects of the process variables like the percent reduction in height (%r) and the height to diameter ratio (H/D). The important observations are as follows. It is obvious that the upsetting load and the values of the normal contact stress increase with %r. However, the pattern of the normal contact stress distribution along the interface doesn't change much with %r. The pattern does not change much with a change in H/D ratio also. However, the values of normal contact stress decrease with H/D ratio and, as a result, the upsetting load also decreases but only to some extent.

CENTRAL LIBRARY
I. I. T., KANPUR
Acc. No. A 193731

Along the interface, the normal stress increase with the radial coordinate. When a full sticking condition is used, the normal stress tends to infinity at the edge. This, of course, is not realistic. Therefore for better modelling of the process, the interfacial slip should be accounted for.

The size of the plastic zone is determined using the contours of effective stress. The plastic zone first appears at the center and at the edge of the die-workpiece interface. With increase in %r, these two regions spread and join. But even at as high value of %r as 20, the region at the center of the interface remains elastic. Only at very high %r, the full region becomes plastic. The size of the plastic zone reduces with H/D ratio but only by a small amount. As for as the pattern of effective stress distribution is concerned, it changes with H/D ratio but not with %r.

The deformation pattern is studied with the help of deformed mesh and the contours of the effective strain. The bulge of the free surface becomes larger when either %r or H/D ratio is increased. However, the effect of H/D is small. When a full sticking condition is used, the phenomenon of the fold-over of the free surface is observed for %r > 20 or H/D < 1. The pattern of effective strain distribution doesn't change much either with %r or H/D ratio. However, the values of effective strain increase with %r and decrease with H/D ratio.

The influence of strain hardening is analysed by obtaining the results for two materials namely aluminium and steel. The values of the normal contact stress, the upsetting load and the effective stress, of course, larger for steel than for aluminium. However, the patterns of the normal contact stress distribution along the interface, the variation of upsetting load with % r and the effective stress distribution are not different. It implies that strain hardening has no effect on these three parameters. It is observed that the bulge profile as well as the values and distribution pattern of effective strain also do not depend on strain hardening.

The important conclusions are :

- Along the interface, the normal stress increases with radial coordinate. When a full sticking condition is used, the normal stress at the edge acquires a non-

realistic value of infinity. Therefore, for realistic modelling of the process, interfacial slip should be incorporated.

- When a full sticking condition is used, the phenomenon of the fold-over of the free surface is observed for %r > 20 or H/D < 1. This, again, doesn't happen in a real-life upsetting process.
- The H/D ratio doesn't seem to have much influence on the process parameters.
- The deformation (i. e. the bulge profile and the values and the distribution pattern of effective strain doesn't get affected by strain hardening.
- Strain hardening has no effect on the pattern of normal contact stress distribution, the variation of upsetting load with %r and the effective stress distribution.

The following works may be taken up as extensions of the present study :

1. Proper modelling of interfacial friction and slip.
2. Dependence of strain rate (viscoplasticity) and temperature on material behavior.
3. Analysis and prediction of defects in the upsetting process.
4. Warm upsetting process.

Bibliography

[1] Prandtl, L., (1923) "Anwendungsbeispiele zu enim Henckyschen Satz über das Plastiche Gleichgewicht," Zeitschrift für Angewandte Mathematik und Mechanik, vol.3, pp. 401-406.

[2] Hill, R., Lee, E. H. and Tupper, S. J., (1951) "A Method of Numerical Analysis of Plastic Flow in Plane Strain and Its Application to the Compression of a Ductile Material between Rough Plates," Journal of Applied Mechanics, vol.18, Trans. ASME, vol. 73, pp. 46-52.

[3] Green, A. P., (1951) "A Theoretical Investigation of the Compression of a Ductile Material between Smooth Flat Dies," Philosophical Magazine, series 7, vol. 42, p. 900.

[4] Shabaik, A., "Prediction of the Geometric Changes of the Free Boundary during Upsetting by the Slip-line Theory," ASME paper no. 70-WA/prd-17.

[5] Hoffman, O. and Sachs, G., (1953) "Introduction to the Theory of Plasticity for Engineers," McGraw-Hill Book Company, New York.

[6] Altan, T., (1971) "Computer Simulation to Predict Load, Stress and Metal Flow in an Axisymmetric Closed-Die Forging" in metal forming, ed. Hoffmanner, A. L., pp. 325-347, Plenum Press.

[7] Prager, W. and Hodge, P. G., (1951) "Theory of Perfectly Plastic Solids," John Willy, New York.

[8] Drucker, P. C., (1954) "Coulomb Friction, Plasticity and Limit Loads," J. Appl. Mech., vol. 21, pp. 71-74.

[9] Kudo, H., (1960) "Some Analytical and Experimental Studies of Axi-symmetric Cold Forging and Extrusion-I and II," Int. Mech. Sci., vol-2, pp. 102-127.

[10] Kudo, H., (1960) "An Upper Bound Approach to Plane-Strain Forging and Extrusion-I and II," Int. J. Mech. Sci., vol 1, pp. 57-83.

[11] Avitzur, B., (1968) "A Metal Forming: Process and Analysis," McGraw Hill Book Company, New York.

[12] Kobayashi, S., (1964) "Upper Bound Solution of Axisymmetric Forming Problems, Parts I and II," Trans. ASME, ser. B, vol. 86, no. 4, pp. 326-332.

[13] MacDonald, A. G., Kobayashi, S. and Thomsen, E. G., (1960) "Some Problems of Press Forging Lead and Alumininum," Trans. ASME, ser. B, vol. 82, pp. 246-252.

[14] Kobayashi, S. and Thomsen, E. G., (1959) "Approximate Solutions to a Problem of Press Forging," Trans. ASME, ser. B, vol. 81, pp. 217-227.

[15] Kobayashi, S. and Thomsen, E. G., (1965) "Upper and Lower Bound Solutions to Axisymmertic Compression and extrusion Problems," Int. J. Mech. Sci., p. 127.

[16] Liu, J. Y., "An Analysis of the Forging of a Flat Ring," ASME paper, no. 70-WA/Prod-28.

[17] Lee, C. H. and Kobayashi, S., (1973) "New Solutions to Rigid-Plastic Deformation Problems using a Matrix Method," Trans. ASME, J. Engr. for Ind., vol. 95, p. 865.

[18] Shah, S. N., Lee, C. H. and Kobayashi, S., (1974) "Compression of Tall, Circular, Solid Cylinders between Parallel Flat Dies," Proc. Int. Conf. Prod. Engr., Tokyo, p. 295.

[19] Chen, C. C. and Kobayashi, S., (1978) "Rigid-Plastic Finite Element Analysis of Ring Compression: Applications of Numerical Method of Forming Processes," ASME, AMD, vol. 28, p. 163.

[20] Oh, S. I. and Kobayashi, S., (1976) "Workability of Aluminium Alloy 7075-T6 in Upsetting and Rolling," Trans. ASME, J. Engr. for Ind., vol. 98, p. 800.

[21] Lee, C. H. and Kobayashi, S., (1971) "Analysis of Axisymmetric Upsetting and Plane-Strain Side-Pressing of Solid Cylinders by the Finite Element Method," Trans. ASME, J. Engr. for Ind., vol. 93, p. 445.

[22] Maccarini, G., Giardini, C., Pellegrini, G. and Bugini, A., (1991) "The Influence of Die Geometry on Cold Extrusion Forging Operations: FEM and Experimental Results," Journal of Materials Processing Technology, vol. 27, pp. 227-238.

[23] Hartely, P., Sturgess, C. E. and Rowe, G. W., (1980) "Influence of Friction on the Prediction of Forces, Pressure Distributions and Properties in Upset Forging," Int. J. Mech. Sci., vol. 22, pp. 743-753.

[24] Hartely, P., Sturgess, C. E. and Rowe, G. W., (1979) "Friction in Finite Element Analysis of Metal Forming Processes," Int. J. Mech. Sci., vol. 21, pp. 301-311.

[25] Bathe, K. J., Ramm, E. and Wilson, E. L., (1975) "Finite Element Formulations for Large Deformation Dynamics Analysis," Int. J. Num. Meth. Engn., vol. 9, pp. 353-386.

[26] Carter, W. T., Jr and Lee, D., (1986) "Further Analysis of Axisymmetric Upsetting," Trans. ASME, J. Engr. for Ind., vol. 108, pp. 198.

[27] Owen, D. R. J. and Hinton, E., (1980) "Finite Elements in Plasticity: Theory and Practice," Pineridge Press, Swansea, UK.

[28] Chakrabarty, J., (1987) "Theory and Plasticity," McGraw-Hill Book Company, Singapore.

[29] Hill, R., (1950) "The Mathematical Theory of Plasticity," Clarendon Press, Oxford.

[30] Crisfield, M. A., (1987) "Consistent Schemes for Plasticity Computation with Newton-Raphson Method," Computational Plasticity Part-I, Owen, D. R., Hinton, E. Onate edited, pp. 133-159.

[31] Dadras, P. and Thomas, J. F. Jr., (1983) "Analysis of Axisymmetric Upsetting Based on Flow Pattern Observations," Int. J. Mech. Sci., vol. 25, no. 6, pp. 421-427.

[32] Nagamatsu, A., Murota, T. and Jimma, T., (1971) "Non-Uniform Deformation of Block in Plane-Strain Compression Caused by Friction (Part-3)," Bulletin of JSME, vol. 14, no. 70, pp. 314-321.